Universal Journal of Catalysis Science
https://ojs.wiserpub.com/index.php/UJCS/

Research Article

Transformation of Styrene Oxide on Bi-Functional Ni, Co and Cu Catalysts Supported on Zirconia-Alumina: Effect of Depositing Zirconia on Alumina

Ruhi H. Pathan[1], Chetan K. Modi[2], Arun G. Basrur[1,*]

[1]Research & Development Centre, Sud-Chemie India Pvt. Ltd. Nandesari, Vadodara-391340, Gujarat, India
[2]Applied Chemistry Department, Faculty of Technology & Engineering, The Maharaja Sayajirao University of Baroda, Vadodara-390001, Gujarat , India
Email: arunbasrur@rediffmail.com

Received: 9 November 2022; **Revised:** 30 November 2022; **Accepted:** 1 December 2022

Abstract: 2-phenyl ethanol (2-PEA) and 2-phenylacetaldehyde (PAA) are important perfumery chemicals which are prepared by hydrogenation and isomerization of styrene oxide (SO) respectively. Activities of Ni, Co and Cu supported on a set of zirconia-alumina supports with varying ZrO_2:Al_2O_3 molar ratio are compared for these reactions. Zirconia was deposited on γ-alumina by deposition-precipitation. All catalysts were characterized by XRD, NH_3-TPD, H_2-TPR, N_2 physisorption, XPS and Raman spectroscopy. Increasing the zirconia content significantly influenced catalyst characteristics. These are correlated with reactivity: i) surface concentration of Ni, Co and Cu (XPS) decreased, which affected conversion of styrene oxide and selectivity to 2-PEA ii) 1 1 1 plane of Cu (XRD) was suppressed which enhanced selectivity of styrene by-product relative to 2-PEA iii) acidity (NH_3-TPD) decreased, which adversely affected yield of PAA. Product space time yields (STY) of 2-PEA and PAA correlated well with surface concentration of active metals (XPS) and acidity (NH_3-TPD) respectively. Various by-products were identified. Styrene appeared to form by deoxygenation of SO. TPR and Raman spectroscopy indicated strong interaction of Co and Ni with alumina while Cu showed strong interaction with zirconia. This reflected in their XRD crystallite size. Cu has different electronic properties than Co and Ni, which reflected in differences in their behavior. This study directly compares the performance of these transition metals in continuous flow studies and correlates catalyst characteristics with reactivity.

Keywords: 2-phenyl ethanol, 2-phenylacetaldehyde, hydrogenation, isomerization, zirconia-alumina composites, acid-base function, metal function, non-noble metal, styrene oxide

1. Introduction

2-phenylacetaldehyde (PAA) and 2-phenyl ethanol (2-PEA) are important perfumery chemicals with floral aroma and fruity flavor. 2-PEA can be synthesized by Friedel Crafts alkylation of benzene with ethylene oxide [1] or Grignard synthesis followed by base hydrolysis [2]. These routes are hazardous and generate waste which is difficult to dispose.

PAA can be prepared by the isomerization of styrene oxide (SO) [3-13] on SiO_2, SiO_2-Al_2O_3, SiO_2-ZrO_2, Al-SBA-15, hydrotalcites, rare earth phosphates, KF supported on alumina, heteropoly acids, neat and modified zeolites such as ZSM-5, BEA and TS-1, Cr-pillared montmorillonite. Weak Lewis acids are reported to be desirable for this

DOI: https://doi.org/10.37256/ujcs.1120232147

reaction [5]. Psaro et.al. [3] have studied silica, silica-alumina and silica-zirconia. They report that incorporation of zirconia even in small concentrations affects the productivity of Si-Zr catalysts for PAA. Specific composition as well as acid-base character of the oxide catalyst are important for isomerization of SO to PAA. Use of bi-component zirconia-alumina is not reported in literature for this reaction.

2-PEA can be prepared by hydrogenation of PAA [4, 14] or direct hydrogenation of styrene oxide, which are ecofriendly routes. Raney Nickel [15-17] catalyst is reported for the latter. It requires addition of a base to improve product selectivity. This is undesirable from generation and disposal of waste effluent.

Noble metals, Pd or Pt supported on carbon, alumina, silica, silica-alumina, silica-zirconia, saponite and titania are reported in literature for the hydrogenation of SO to 2-PEA [3, 18-25]. These are mainly batch and few continuous flow reactions. Noble metal based catalysts are highly active and selective for this transformation. The metal content of the catalysts used in these studies ranges from 1 – 3 wt%, which is high. Their high cost is a drawback.

Non-noble metals such as Ni, Co and Cu are significantly cheaper than noble metals (Pd or Pt). They are used for hydrogenation of alpha-beta unsaturated aldehydes to unsaturated alcohols [26-29]. These metals supported on a variety of carriers are reported for the hydrogenation of SO to 2-PEA [3-4, 30-35] mainly in batch reaction and one continuous flow vapor phase reaction. While zirconia-silica is studied [3], zirconia-alumina carriers are not covered.

The acid-base properties of carrier in supported metal catalysts are reported to influence product selectivity for the transformation of SO to 2-PEA. However, there are contradictory results. Bergada et.al. report that addition of basic materials such as MgO favors both conversion of SO and its selectivity to 2-PEA [34]. Kirm et.al. [18-19], who have studied Pd and Pt supported on alumina, charcoal and MgO report that acid-base nature of the carrier influences product selectivity between PAA and 2-PEA, as well as the formation of 1-PEA. They report that Pd or Pt supported on γ-alumina form significant amounts of 1-PEA and PAA, whereas activated carbon support forms PAA as the major product, with some 1-PEA. In contrast, Kanojia et.al. [30] who have studied Ni supported on the same types of carriers as Kirm et.al. report that the carrier plays a passive role.

Further, most of these studies are fragmented. They differ either in the combination of transition metal and carrier used or reactor type or reaction conditions, and hence do not enable direct comparison of performance between these three transition metals on an equitable basis. They comprise Ni or Co or Cu supported on diverse carriers such as Nickel on Saponites [32], Nickel on alumina, MgO and Carbon [30], Cu on SiO_2 or silica-alumina or silica-zirconia [3], unsupported nanocrystalline Ni [31], Ni and Co on layered double hydroxides [4], Ni on MgO [34], Cu on pentasil type borosilicate or aluminosilicate zeolites or silico-aluminophosphate [33]. Reaction conditions and reactor type too differ between these studies. Most of the studies are batch reactions [3-4, 17, 30-32, 34] and few continuous flow reactions [33, 18-19]. The advantage of flow reactor is higher productivity, ease of operation and lesser downtime.

The formation of by-products is reported in some studies [3-4, 19, 30-31, 33, 36-39]. These constitute styrene, ethylbenzene, toluene, 2-methyoxy-2-phenylethanol, 1,3,5 triphenylbenzene and trimers of phenylacetaldehyde.

The objective of the present work is to study Ni, Co, Cu based catalysts on a common set of carriers and preparation and evaluation conditions to enable equitable comparison. Further, while all three elements belong to the first transition series, Cu presents an atypical electronic configuration and its Fermi level does not overlap with the d band. Its effect on reactivity has not been studied so far for this reaction. Use of bi-component zirconia-alumina is not reported for the transformation of SO. Thus, it would be interesting to study these aspects. Fifteen bi-functional catalysts comprising Ni, or Co or Cu supported on a set of 5 zirconia-alumina carriers, with varying mole ratio of zirconia:alumina, are studied. Zirconia is deposited on γ-Al_2O_3 by deposition precipitation. The zirconia:alumina content is varied systematically to influence acid-base properties and possibly metal-support interactions. The zirconia-alumina carrier is prepared from learning of an earlier study published by us [40] wherein a detailed description of the chemical composition of the as synthesized zirconia-alumina carrier and its effect on acid-base behavior in the transformation of 2-methyl-3-butyn-2-ol is reported.

The catalyst performance is determined in a continuous flow reactor. The influence of metal function and acid-base function on conversion and product selectivity for transformation of styrene oxide is compared for these catalysts. Trends are studied for both the main reactions as well as major side reactions. The reactivity of the catalysts is correlated with their physico-chemical characteristics and electronic properties of the three metals.

2. Experimential

2.1 *Materials*

Zirconyl Nitrate solution (12.4wt% as Zr) and Sodium carbonate (99.9%) were purchased from M/s SD Fine Chemicals, India. Aluminum monohydrate (99 wt. % purity) was obtained from Sud-Chemie India Pvt. Ltd., Vadodara, India. It was calcined at 550°C for 8 hours to form γ-alumina. $Ni(NO_3)_2.6H_2O$, $Co(NO_3)_2.6H_2O$ and $Cu(NO_3)_2.3H_2O$ were obtained from Merck.

2.2 *Support Preparation*

200 g Zirconyl nitrate solution (16.8 wt% ZrO_2) was taken in a beaker. 184 g demineralized water and 83 g γ-alumina (d50 8 μm) were added with stirring. The mixture was heated to 70°C. Zirconia was precipitated by adding 2N sodium carbonate solution (5 ml/min) to a final stable pH of 9±0.1. The precipitate was aged in the mother liquor at 70 °C for 1 h. The precipitate was recovered by filtration and washed with hot demineralized water (80 °C), followed by overnight drying at 120 °C (8h) and calcination in a flow of air at 550 °C for 4 h. The alumina and zirconia contents of the filtrate were < 200 ppm each, indicating almost quantitative precipitation of zirconia and negligible dissolution of the γ-alumina. The resultant solid had a nominal molar composition ZrO_2:Al_2O_3 0.25:0.75.

Solids with ZrO_2:Al_2O_3 molar ratios 0.5:0.5 and 0.75:0.25 were prepared using the method described above. The actual compositions of the carriers determined by ICP analysis and their nomenclature are given in Table 1 below.

The sample of pure ZrO_2 was prepared by the same method as described above but without including γ-alumina powder. The average particle size of the powders increased from d50 20 μm to 70 μm with increasing content of zirconia.

The above samples, including one of pure γ-alumina were used as carriers for the preparation of Co, Ni and Cu supported metal catalysts.

2.3 *Catalyst Preparation*

Supported metal catalysts were prepared by the incipient wetness method. An aqueous solution of the metal nitrate, equivalent in volume to the water pore volume of the carrier was heated to 65 °C and added to the carrier to achieve a nominal metal content of 12 wt% in the final catalyst. Contents were aged at ambient conditions for 30 minutes before drying at 120 °C and further calcining in air at 500 °C, 4h. The resultant catalysts were named M-ZA ## where M stands for one of Co, Ni or Cu and ZA ## stands for the nominal mole percent of zirconia in the zirconia-alumina bi-component carrier. The composition of the catalysts was determined by ICP analysis. Average metal content across all the catalysts was 11.7 wt% and standard deviation was 1.146 for a nominal metal content of 12 wt%. Actual composition is given in Table 1 where the active metal contents are expressed as their oxides, (NiO, Co_3O_4 and CuO) based on identification by XRD. Abbreviations and composition of the catalysts (in oxide form) is given in Table 1 below.

Table 1. Nomenclature and actual composition of the carriers and catalysts determined by ICP analysis

Catalyst / Carrier Nomenclature	Ni, Co or Cu (as oxide) (wt%)	ZrO_2 (wt%)	Al_2O_3 (wt%)
ZA 100	0.0	100	0.0
ZA 75	0.0	78.4	21.6
ZA 50	0.0	54.7	45.3
ZA 25	0.0	28.7	71.3
ZA 0	0.0	0.0	100
Ni-ZA 100	13.9	86.1	0.0
Ni-ZA 75	13.0	68.2	18.8
Ni-ZA 50	14.3	46.9	38.8
Ni-ZA 25	12.9	25.0	62.1
Ni-ZA 0	14.0	0.0	86.0
Co-ZA 100	14.3	85.7	0.0
Co-ZA 75	17.3	65.1	17.7
Co-ZA 50	17.7	45.2	37.1
Co-ZA 25	15.4	24.5	60.1
Co-ZA 0	14.8	0.0	85.2
Cu-ZA 100	15.5	84.5	0.0
Cu-ZA 75	16.3	65.6	18.1
Cu-ZA 50	16.3	45.8	37.9
Cu-ZA 25	16.9	23.9	59.2
Cu-ZA 0	14.9	0.0	85.1

3. Material Characterization

All the samples are characterized by N_2 physisorption, Powder X-ray diffraction, Inductively coupled plasma analysis (ICP-OES), Temperature Programmed Desorption of ammonia (NH_3-TPD), Temperature Programmed Reduction (H_2-TPR), X-ray photoelectron Spectroscopy (XPS) and Lazer Raman Spectroscopy.

Phase identification is done with a Bruker D8 ADVANCE X-ray diffractometer with a Cu Kα source, wavelength 1.5406 Å. Samples were scanned in 2θ range of 5 to 80° at 2°/ min and a step size of 0.02/s. ICCD PDF4+ X-ray powder diffraction library was used. Metal crystallite size is determined from the Scherrer equation.

A Quantachrome QUADRASORB SI IV is used for measuring BET surface area and pore volume by nitrogen physisorption at liquid nitrogen temperature. Prior to analysis, samples were degassed under vacuum at 300 °C for 3 hours in a Quantachrome Make 'Flovac' degasser.

Chemical composition of the catalysts is determined by ICP OES Thermoscientific iCAP 6000 series. Argon gas was used for generating the plasma. The samples were digested in aqua regia and diluted appropriately for determining the chemical composition.

An Aimil Fotoflame Flame photometer is used to determine the sodium content of the samples.

Ammonia TPD (Temperature Programmed Desorption) and TPR (Temperature Programmed Reduction) are carried out on a Micromeretics AutoChem-II 2920 instrument using a U shaped reactor made of quartz and a TCD detector.

For ammonia TPD, a sample of particle size 20-60 µm is pretreated in flowing helium at 550 °C, followed by cooling to 50 °C, and saturating with ammonia (5 vol% NH_3 in Helium, 25 ml/min, 30 minutes). The sample is purged with flowing Helium gas for 60 minutes to remove un-adsorbed ammonia. The TPD is done by ramping the temperature from 50 °C to 550 °C at 10 °C/min in a flow of pure helium (25 ml/min).

The TPR experiments are done in a similar manner as TPD by pretreating the calcined samples of the catalysts in a flow of pure Helium at 120 °C for 60 minutes to remove moisture. The sample is then cooled to 25 °C in a flow of Helium gas. The TPR is carried out in a stream of 10 vol% H_2 in N_2 (25 ml/min) by ramping the temperature to 800 °C at 10 °C/

min.

XPS is carried out with a Scienta Omicron ESCA+ make instrument. A monochromatic Al Kα source with hv 1486.6 eV was used as X-ray source.

Lazer Raman spectroscopy is carried out with a Reninshaw inVia Reflex Microscope with a Nd:YAG 532 nm lazer.

4. Catalytic transformation of styrene oxide

The catalytic reaction studies are carried out in continuous flow ½" ID stainless steel reactor heated with a tubular furnace. H_2 is fed with Bronkhorst Mass Flow Controller. Pressure is controlled manually with a Tescom make back pressure regulator. Styrene oxide is fed using a Scientific Systems Inc. HPLC pump. The catalyst is tableted and sized to granules and the fraction between 0.5-0.8 mm is charged to the reactor. The catalyst bed is positioned in the isothermal zone of the furnace with glass beads at upstream and downstream. The catalyst is dried in nitrogen at 150 °C (4h). The nickel and cobalt catalysts are reduced at 500 °C whereas the copper based catalysts are reduced at 400 °C. Basis is reduction profiles of TPR (Figure 3). The reactor is cooled to reaction temperature 150 °C in hydrogen and pressurized to 10 bar g. Styrene oxide is fed along with hydrogen (H_2:Styrene oxide 2.75:1 molar). It was ascertained that this ratio is adequate. WHSV based on styrene oxide is 6 h-1. Run length is 8h on stream with hourly sampling of product.

The product is condensed in a double pipe heat exchanger and collected in a gas-liquid separator. It is analyzed with an Agilent 7890B Gas chromatograph with a 30 m x 0.5 mm Innowax HP capillary column using FID detector and Helium as carrier gas. Retention times and response factors of the components of the feed and product are determined using calibration mixtures.

% Conversion of Styrene oxide is calculated as

$$\text{Conversion \%} = \frac{\text{Concentration of SO in reactant} - \text{SO concentration in product}}{\text{Concentration of SO in reactant}} \times 100$$

Selectivity is calculated in two ways.

The product selectivity based on moles of styrene oxide reacted is calculated by the following equation

$$S_{i/SO} = \frac{\text{Mol component i produced}}{\text{Mol SO converted}}$$

This equation is also used to express product yield.

Relative selectivity between two products formed is calculated as

$$S_{i/j} = \frac{\text{Mol component i produced}}{\text{Mol component j produced}}$$

Where i and j are two products formed from two different reactions within the reaction network.

The latter method of calculating selectivity is very useful when there is a network of reactions such as in scheme 1 (Figure 8 below). It provides means of comparing between reactions.

5. Results and Discussion

5.1 *Catalyst Microstructure*

BET specific surface area and pore volume of the catalysts are shown in Figure 1 below. Values of specific surface areas are shown by bars in light color with values on primary Y axis and values of pore volume are shown by bars in dark color with values on secondary Y axis.

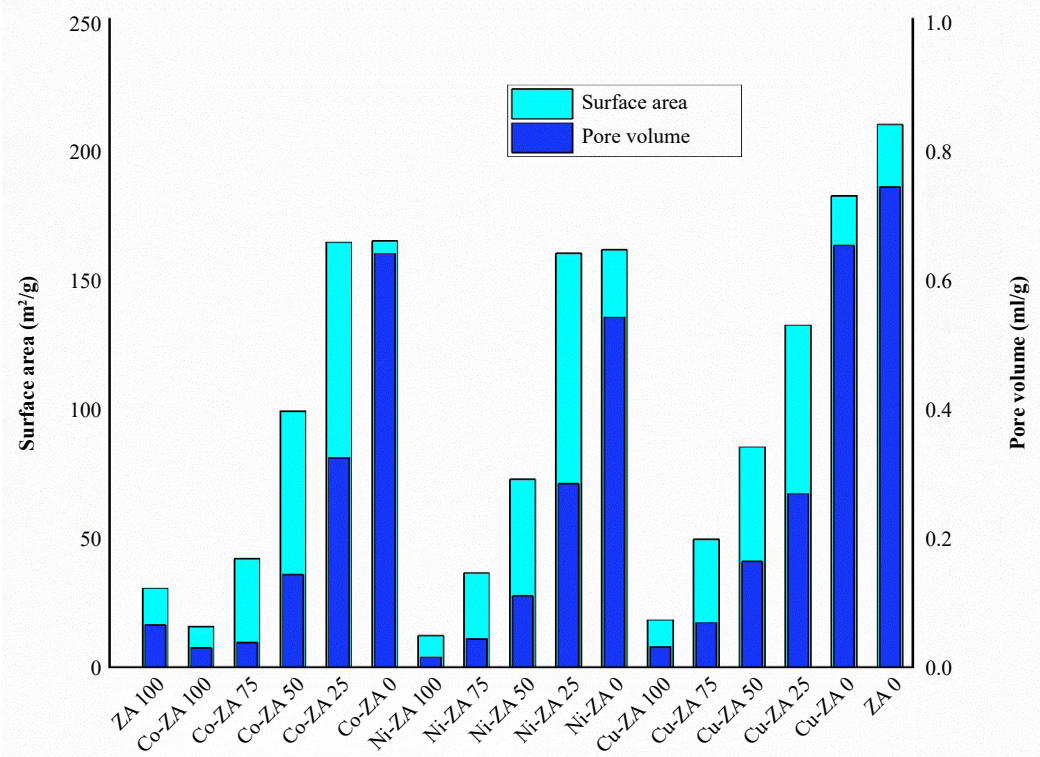

Figure 1. BET specific surface area and pore volume of the catalysts by Nitrogen physisorption

As seen from this Figure the zirconia carrier (ZA 100) has very low specific surface area and pore volume. The precipitate was gel-like in nature and shrank during drying thereby decreasing surface area and pore volume. Both these parameters improve significantly in samples prepared by deposition of zirconia on γ-Al_2O_3. Thus deposition-precipitation lends this advantage.

All the Ni based catalysts show slightly lower specific surface area than their Co or Cu counterparts for a given support.

Pore size of the γ-Al_2O_3 substrate is 13.8 nm. It initially decreases sharply to 3.6 nm and then progressively to 3.3 nm and 2.4 nm with increasing zirconia content. The sample of neat zirconia (ZA-100) showed pore diameter 2.0 nm. Thus, all the samples are mesoporous. Isotherms are type IV with clear hysteresis (not shown in the paper).

5.2 *X-ray Powder Diffraction*

The catalysts were subjected to powder XRD and the crystallite sizes of the oxides of Co, Ni and Cu determined by Scherrer equation are presented in Figure 2. The diffractograms are presented in Figure A1. Phases detected are NiO (JCPDS 04-006-1773), Co_3O_4 (04-007-2519), CuO (Tenorite 00-002-1040), ZrO_2 (Tetragonal 00-050-1089) and Aluminum oxide (gamma 00-010-0425). The crystallite size of Cobalt oxide is determined from the d_{311} plane, that of Ni oxide from d_{200} and that of Cu oxide from d_{111}, which correspond to the most intense peaks of these samples in the XRD diffractogram.

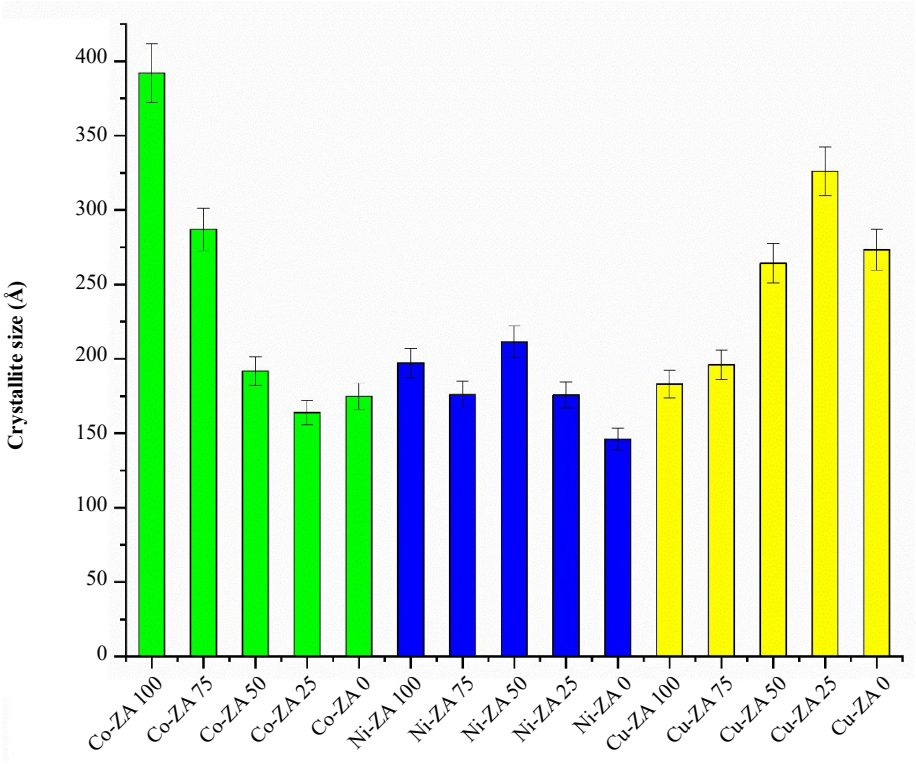

Figure 2. Crystallite size of metal oxides of Co, Ni and Cu determined from powder XRD by Scherrer equation

In general, higher specific surface area of the support provides room for better dispersion of active metals in supported metal catalysts. Further, stronger metal support interactions minimize the possibility of sintering of the active metal precursors during calcination. From Figure 2, it is observed that the crystallite size of Co_3O_4 decreases significantly with decreasing zirconia content of the carrier. NiO shows a similar trend but to a smaller extent. This indicates improvement in dispersion with decreasing zirconia in the carriers in both cases. This also coincides with increasing specific surface area. Both Co and Ni catalysts show this trend. As seen from the results of TPR (Figures 3 a, b) both Co and Ni show stronger interaction with alumina support. Thus, their behavior is in line with the general expectation from MSI (Metal support interaction). CuO however shows a clear opposite trend. Dispersion of Cu is higher on supports which are rich in zirconia, which have considerably lower specific surface area. The reason for this is attributed to stronger interaction of CuO with zirconia (Figure 3c. TPR), which prevents sintering during calcination. Thus, metal support interaction has a stronger influence on crystallite size of copper catalysts of this work than specific surface area of the support material.

The relative intensities of XRD peaks for Co and Cu catalysts are compared with the JCPDS reference value (column "relative intensity of hkl plane (Ir)") in Table 2 below.

Table 2. Trend of relative intensity of XRD peaks for Co, Ni and Cu catalysts

Catalysts	XRD phase	JCPDS No	Miller Index	Relative intensity of hkl plane (Ir)	Relative Intensity in X-ZA# series samples (Ir)				
			hkl		ZA-100	ZA-75	ZA-50	ZA-25	ZA-0
Co-series catalysts	Co_3O_4	04-007-2519	200	32	60	77	48	35	29
Ni-series catalysts	NiO	04-006-1773	111	64	58	57	60	79	112
Cu-series catalysts	CuO	00-002-1040	111	99	51	60	86	81	87

As seen from Table 2, preferential orientation of crystal planes is observed for Co and Cu catalysts which are rich in zirconia. The 2 0 0 plane of cobalt catalysts (Co-ZA-100 and Co-ZA-75) supported on carrier with ≥50 mol% zirconia is 1.5 to 2.4 times more intense than that of the JCPDS reference relative intensity of this peak. The relative intensity of the 1 1 1 plane is significantly subdued (0.5-0.6 the intensity of JCPDS reference value) in the case of Copper catalysts, Cu-ZA-100 and Cu-ZA-75, which are supported on carriers with ≥ 75 mol% zirconia. The intensity of 1 1 1 plane of Ni catalysts increases when γ- Al_2O_3 content in the carrier ≥ 75 mol%. But this appears to be due to contribution from the 3 1 1 plane of γ- Al_2O_3 which is a broad peak at 2-θ 37.604°, which is very close to the Ni 1 1 1 peak. Thus, the possibility of preferred orientation in Ni catalysts is deemed absent.

The catalysts which are reduced with H_2 show similar characteristics, and these are correlated with reactivity in Figure 13c.

5.3 *Temperature Programmed Desorption of ammonia*

NH_3 TPD profiles of supports are presented in Figure A2. NH_3 TPD profiles of Co, Ni and Cu supported catalysts are presented in Figure A3. As seen from Figure A2 all the supports show weak and strong acidity. The peak at about 100 °C is due to physisorbed NH_3 and the one at about 300 °C is due to chemisorbed NH_3. The latter peak is relevant to acidity and hence responsible for reaction. Acidity increases with increasing alumina content (Figure A2 and Figure A3). Acid strength also increases with alumina content of support as evidenced by shift of the peaks to higher temperatures (Figure A2).

As seen from Figure A3, the supported catalysts retain the characteristics of the supports. They too show weak and strong acidity largely in the same range of temperature as the supports. The fraction of strong acidity is higher in the catalysts compared to the supports. Further, catalysts supported on neat alumina (ZA 0) show highest acidity and higher acid strength. Catalysts with 25 mol% ZrO_2 in their supports show comparatively lower acidity, which is however, significantly higher than that of the remaining catalysts which have ≥50 mol% ZrO_2.

Values of acidity are provided in Figure A4 a, b (Cobalt catalysts), c (nickel catalysts), d (Copper catalysts). As seen from this figure the strong acidity of supports increases with increasing alumina content till 50 mol% after which it tends to flatten out. In contrast the strong acidity of catalysts increases continuously with alumina content indicating some contribution from the active metal component. Trend for strong acidity of catalysts supported on neat alumina (ZA 0 series) is Co > Cu > Ni. Trend for catalysts with 25 mol% ZrO_2 is Co>Ni>Cu. Catalysts containing ≥50 mol% zirconia do not show specific trends.

Further, from Figure A4 b, c, d it is observed that the quantity of ammonia adsorbed ranges from 0.126 – 0.149 mmol/g catalyst when the support is neat zirconia (ZA 100), whereas it is 3-4 times higher (ranging from 0.404 – 0.526 mmol/g catalyst) when the support is neat alumina (ZA 0).

Thus, acidity is dependent on the combination of active metal and carrier composition. These differences in acidity manifest themselves in trends of product selectivity in the transformation of styrene oxide, which is discussed in a subsequent section of this paper.

5.4 *Temperature Programmed Reduction*

TPR Profiles of Co, Ni and Cu oxides supported on the carriers with varying zirconia: alumina content are shown in Figures 3 a, b, c.

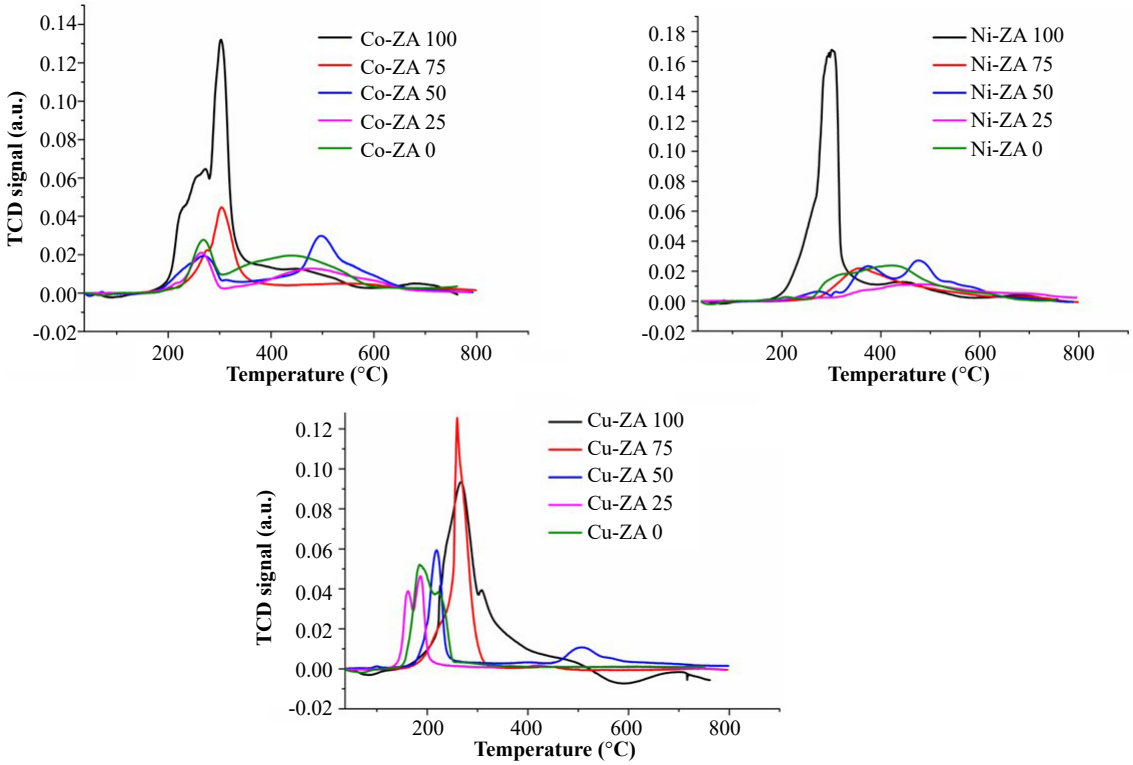

Figure 3. TPR profiles of a) Co-catalysts b) Ni-catalysts and c) Cu-catalysts supported on different supports

The following distinguishing features are observed from Figure 3a, b, c:

Figure 3a, 3b and 3c show clear demarcation of reduction profile for the catalysts prepared with carrier containing ZrO2 ≥ 75 mole%, and for the carriers where ZrO_2 < 75 mole%. Referring Figure 3a, cobalt catalysts supported on alumina rich carriers i.e. ZA 50, ZA 25 and ZA 0 show two distinct peaks, one at lower temperature around 275 °C and a broad second peak with maxima between 400-600 °C. This indicates two type of cobalt species on alumina rich carriers or stage-wise reduction of Co_3O_4 to CoO and further to Co(0). This is consistent with reports in literature [41]. The cobalt catalysts which are prepared on zirconia rich carriers (≥75 mol%) show only one intense peak at ~300-304°C with an ascending shoulder. This is attributed to reduction of Co_3O_4 with poor interaction with support (similar to unsupported Co3O4). This is consistent with reports in literature [42].

Reduction profiles of nickel based catalysts (Figure 3b) are more diffuse and broad peaks range from 250 °C to 600°C, which can be attributed to nickel oxide dispersed on alumina. Ni-ZA 0 and Ni-ZA 25 show reduction peaks at temperature >400°C indicating strong metal support interaction. Ni-ZA 50 shows two distinct peaks at about 390° and 490°C respectively, indicating two different nickel species. Ni-ZA 75 shows a single peak ~390 °C which is at lower temperature than Ni-ZA 50. Ni-ZA 100 shows a single intense peak at 300 °C indicating least metal support interaction (with zirconia).

The comparison between nickel and cobalt based catalysts suggests that cobalt has relatively stronger interaction with zirconia while nickel has stronger interaction with alumina. Behavior of copper based catalyst is contrary to that of nickel catalysts. The copper catalysts (Figure 3c) show bidentate peaks with their Tmax at temperature <225 °C. This is attributed to stage-wise reduction of Cu(II) to Cu(I) and then to Cu(0). Copper catalysts supported on alumina rich carriers i.e. ZrO_2 < 50 mole% show lower TPR maxima than when copper is supported on zirconia rich carriers, indicating weaker metal support interaction of Copper with alumina than zirconia. This is well co-related with crystallite size of copper based catalysts which show reverse trend than Co and Ni catalysts for ZA 0 and ZA 75 supports.

All three catalysts Co-ZA 50, Ni-ZA 50 and Cu-ZA 50 which are supported on carries containing 1:1 molar ZrO_2:Al_2O_3 present two well separated reduction peaks, which is different from the remaining catalysts. There appear to be two distinct types of metal-support interactions with zirconia and alumina respectively for this set.

Ni-ZA 100, Co-ZA 100 and Cu-ZA 100 prepared with neat zirconia carrier show a single peak of high intensity which has ascending or descending shoulders. The intensity of this peak is 3 – 8 times that of the peaks of catalysts prepared using the remaining carriers. As shown in Figure 4 below, this is attributed to spillover of hydrogen to the support.

The ratio of the quantity of H_2 experimentally consumed in TPR and the theoretical quantity required for complete reduction of NiO, Co_3O_4 and CuO to the metal is shown in Figure 4 below for all the catalysts.

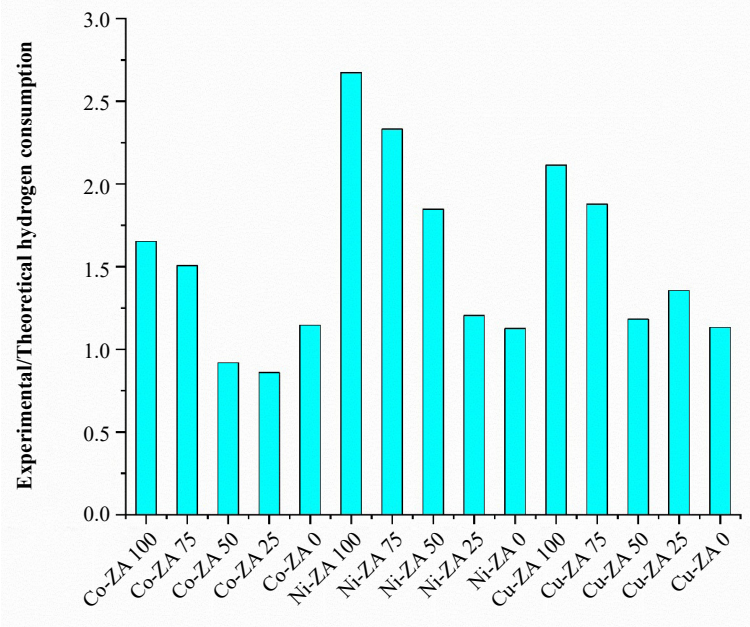

Figure 4. Ratio of experimental hydrogen consumption to theoretical consumption in TPR analysis

As seen from Figure 4 the ratio of experimental to theoretical hydrogen consumption is significantly greater than 1 for most of the catalysts with zirconia content > 50 mol%. It tends to decrease with decreasing zirconia content of the catalyst /and approaches values closer to 1.

Pure zirconia carrier ZA 100 shows very low consumption of hydrogen, a mere 0.4 mmol/g cat (not shown in Figure 4) compared to 2.07 - 4.96 mmol/g cat for the remaining samples. The direct reduction of zirconia by hydrogen at elevated temperature is reported to be very difficult even at very severe conditions such as 2500 °C [43]. Thus the small hydrogen uptake observed in ZA 100 could be due to presence of impurity metal oxides which are reducible at the conditions of the TPR studies.

Spillover of hydrogen from metal to zirconia is reported for Pt/ZrO_2 [44] and Cu/ZrO_2 [45]. Spill-over of hydrogen from Ni-Ga alloy and their intermetallic compound to SiO_2 carrier is also reported [46].

Thus, the excess hydrogen uptake observed in the current studies is attributed to spillover of hydrogen from the metals to the carrier.

5.5 *X-ray Photoelectron Spectroscopy studies*

The results of XPS studies of Co, Ni and Cu supported on ZA100 (neat zirconia) and ZA-0 (neat γ- Al_2O_3) are shown in Figure 5 a,b,c and Figure 6 a,b,c below. Figure 6d shows XPS of Ni-ZA 50 with a 1:1 molar zirconia:alumina content:

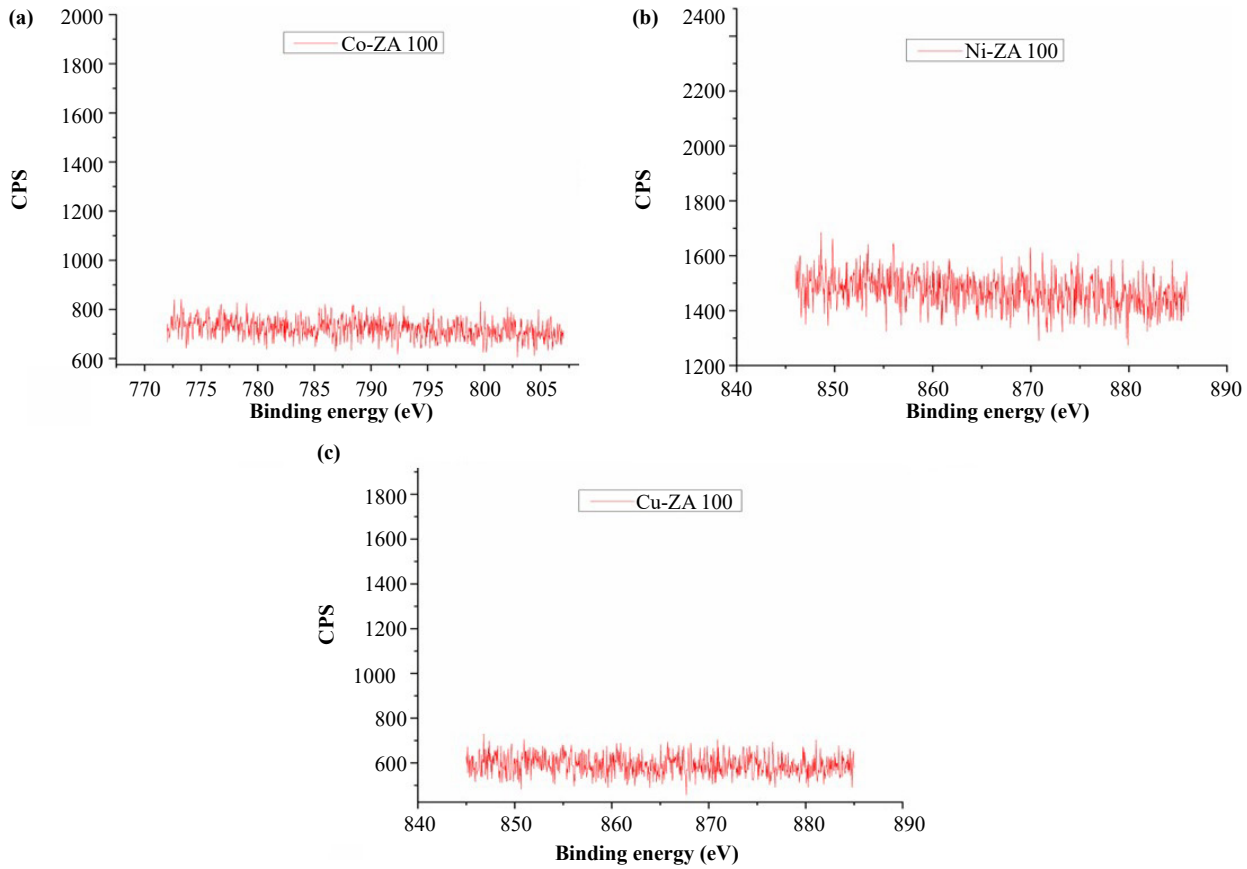

Figure 5. XPS of a) Co-ZA 100, b) Ni-ZA 100 and c) Cu-ZA 100

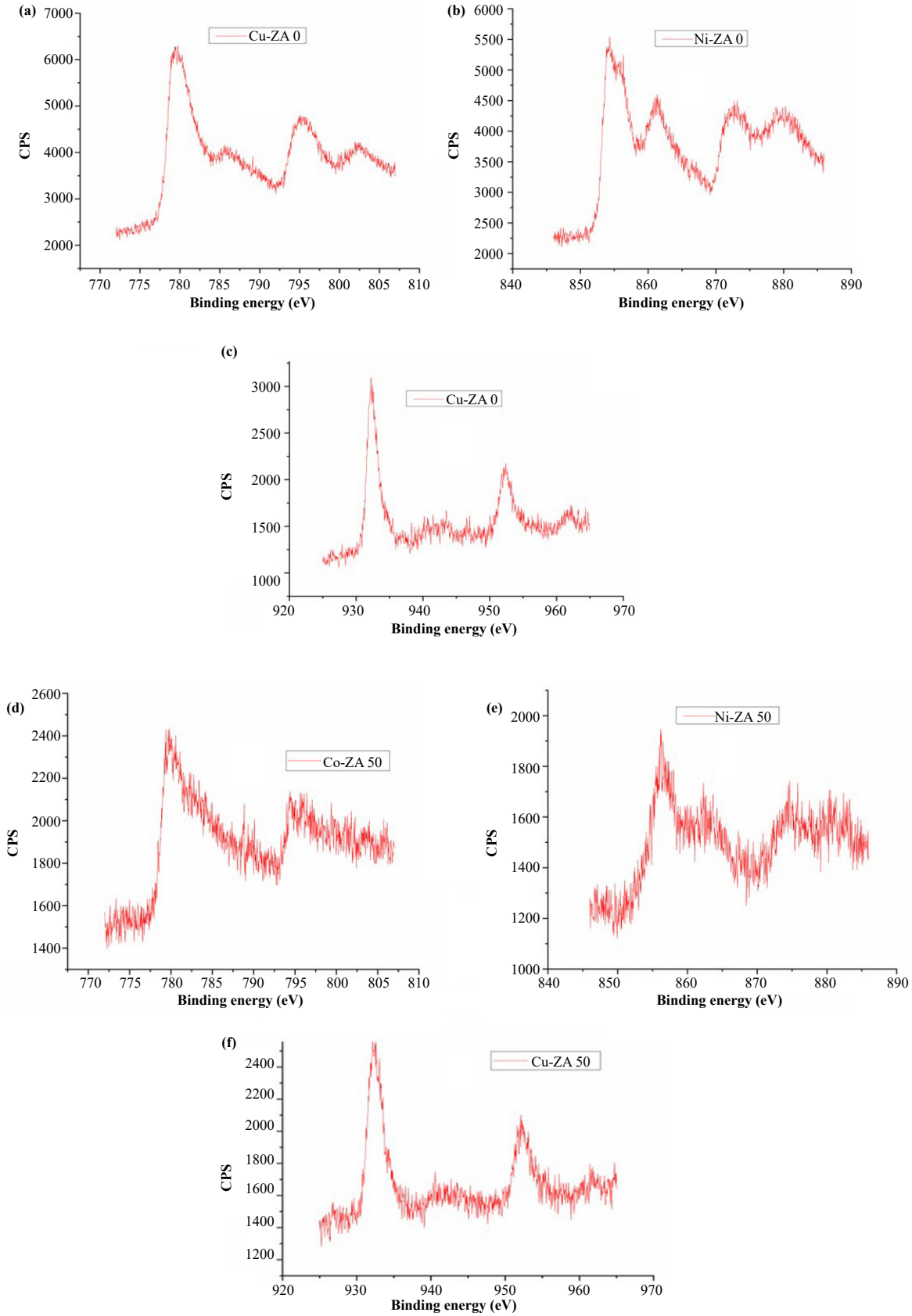

Figure 6. XPS of a) Co-ZA 0, b) Ni-ZA 0, c) Cu-ZA 0; d) Ni-ZA 50,e) Ni-ZA 50, f) Ni-ZA 50

Comparing Figure 5 a, b, c with Figure 6 a, b, c for Co, Ni and Cu supported on neat zirconia and neat alumina respectively it is clear that:

All three active metals Ni (2p3/2 binding energy 854.32 eV), Co (2p3/2 779.37 eV), and Cu (2p3/2 932.24 eV) are clearly seen on the surface of the catalyst when the carrier is neat alumina (Figures 6 a, b, c respectively), whereas they are not detected on the surface when the carrier is neat zirconia (Figures 5 a, b, c respectively).

Ni-ZA 50 (Figure 6 d) which contains ZrO_2 and Al_2O_3 in 1:1 molar ratio shows a peak of Ni (2p3/2) with relative peak area which is only about 25.6% of that of Ni-ZA 0. Similarly, Cu-ZA 50 shows peak area Cu (2p3/2) which is 23.0% relative to Cu-ZA 0 and Co-ZA 50 shows peak area Co (2p3/2) area which is 23.6% relative to Co-ZA 0. This indicates lower surface concentrations of these metals than on a neat alumina support. Figures of the latter two are not included.

ICP analysis (Table 1) and the other characterization techniques clearly show presence of the active metals in all the catalyst samples close to target value. Hence, the active metals appear to migrate to subsurface layers with increasing content of zirconia in the catalyst. This correlates with the low STY of 2-PEA of zirconia rich catalysts in the conversion of styrene oxide (subsequent sections).

5.6 *Raman spectroscopy*

Results of Raman spectroscopy are shown in Figure 7 below. γ-Al_2O_3 is Raman inactive. t-ZrO_2 is Raman active. Raman shift bands of oxides of Co, Ni, Cu and Zr reported in literature are compiled in Table 3 below

Table 3. Raman transitions of pure metal oxides

Metal oxide	Symmetry	Raman shift bands (cm^{-1})	Reference
NiO	Cubic	440 (1P TO), 560 (1P LO), 730 (2TO), 930-960 (TO+LO), 1030-1080 (2LO)	N. Mironova-Ulmane et.al, Meza Fuentes E. et.al. [47,48]
CuO	Monoclinic	296 (Ag), 346 (Bg), 631 (Bg)	M. Rashad et.al. [49]
Co_3O_4	Cubic	194 (F2g), 482(Eg), 522 (F2g), 618 (F2g), 691 (A1g)	M. N. Iliev [50]
ZrO_2	Tetragonal	155 (B1g), 260 (Eg), 320 (B1g), 460 (Eg), 606 (B1g), 641 (Eg)	Antonina P. Naumenko et.al. [51]

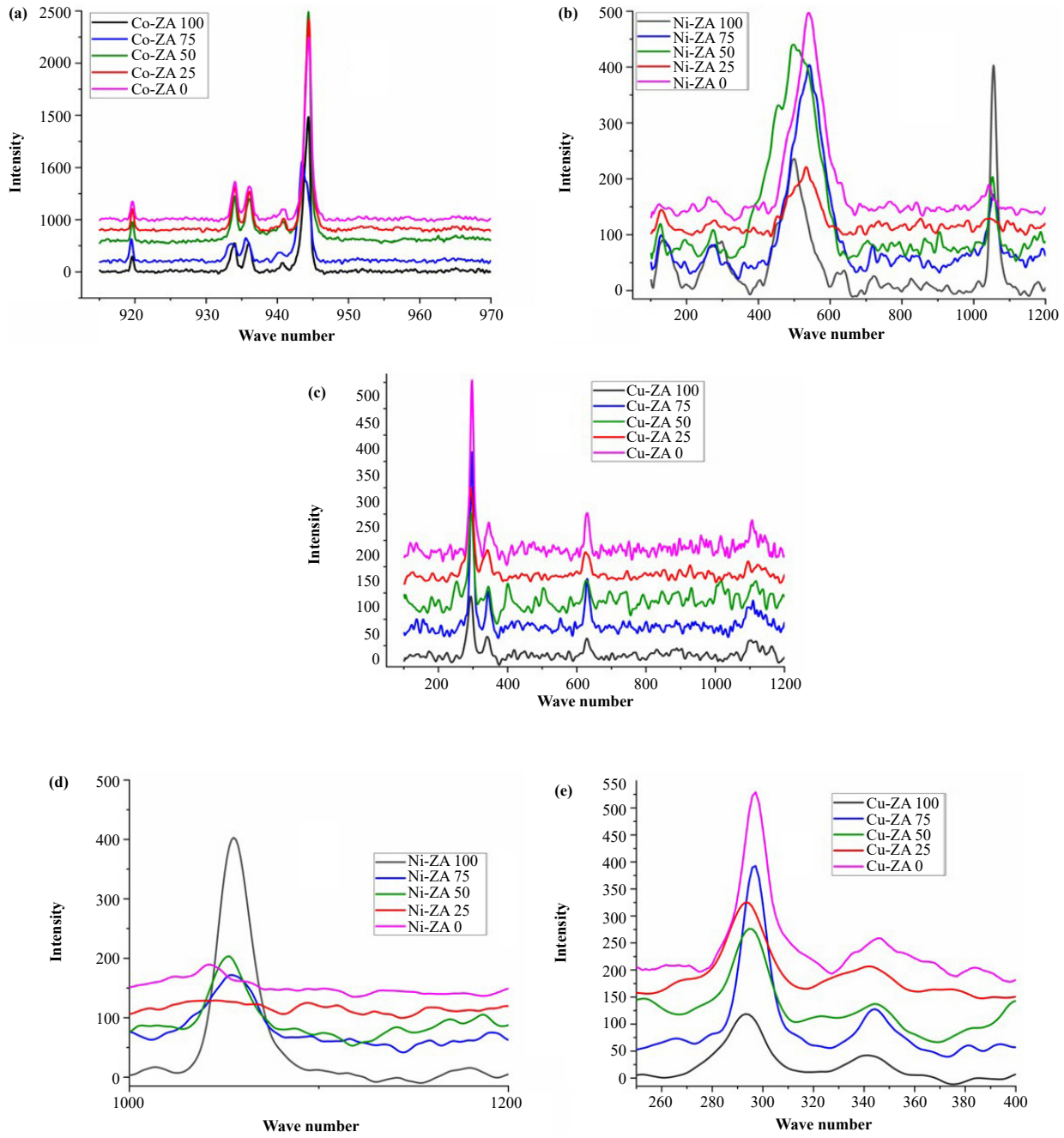

Figure 7. Raman shift bands of a) Co catalysts, b) Ni catalysts c) Cu catalysts supported on zirconia-alumina, d) zoom in image-change in intensity of band of Ni catalysts e) zoom in image-change in intensity of band of Cu catalysts.

The Raman spectra of catalyst samples are shown in Figures 7 a-e.

The following trends are observed by comparing the transitions in Figure 7a-e with the Raman transitions listed in Table 3:

Referring Figure 7a): The supported Co catalysts exhibit all five Raman transitions characteristic of Co_3O_4 spinel(49). The peak in the 522 cm^{-1} region shows a Blue shift of 5 cm^{-1} (from 519 to 524 cm^{-1}) when the support changes from neat zirconia to neat alumina, indicating strengthening of the Co-O bond.

Referring to Figure 7b): All the Nickel catalysts show two transitions one each of 1P LO (497-541 cm^{-1}) and 2P LO (1045-1055 cm^{-1}). The intensity of the latter band decreases with increasing alumina content, changes can be seen

in zoomed Figure 7d. Decrease or disappearance of this band is reported for NiO [47], NiO/Al_2O_3 [52] and for Ni-Al hydrotalcites [48]. The decrease in intensity is attributed to a decrease in crystallite size, metal support interaction or particle size of NiO, all of which reflect in better dispersion. This corroborates with results of XRD which show decrease in crystallite size with increasing alumina in the catalyst. All the Ni catalyst samples show two additional transitions at (275-303 cm^{-1}) and (130-140 cm^{-1}) which are relatively more prominent for samples containing zirconia. These are attributed to tetragonal zirconia. The peak in the 540 cm^{-1} region shows a strong Blue shift of 38 cm^{-1} (507 to 545 cm^{-1}) when the support changes from neat zirconia to neat alumina, indicating strengthening of the Ni-O bond, similar to Co catalysts. TPR too shows stronger MSI of Ni with alumina.

Referring to Figure 7c): All the supported Cu catalysts show all three Raman bands characteristic of CuO (Tenorite). Samples with ≥ 75 mol% zirconia show significantly higher intensity of the band at about 295 cm-1 than the remaining samples of Cu based catalysts (Figure 7e). This correlates with XRD studies which show low relative intensity of the 1 1 1 plane of CuO. Similar effect of 0 0 1 and 1 0 1 orientated polycrystalline SnO films on the intensity of bands of Raman spectra is reported [53]. Contrary to the Co and Ni catalysts, a weak red shift of 2 cm^{-1} (296 to 294 cm^{-1}) is observed for the band at 296 cm^{-1}, indicating weakening of the Cu-O bond as support changes from neat zirconia to neat alumina. TPR also indicates weaker metal support interaction between CuO and Al_2O_3, because maxima of the reduction peak shifts to lower temperature.

5.7 *Catalytic transformation of styrene oxide*

Unreacted styrene oxide (SO), phenylacetaldehyde (PPA), 2-phenyl ethanol (2-PEA), 1-phenyl ethanol (1-PEA) and styrene were the major products. Small quantities of ethylbenzene (EB), toluene and heavies were also identified in the product. Out of these phenylacetaldehyde and 2-phenyl ethanol are valuable products.

The above mentioned products are expected to form from reactions shown in Figure 8 below.

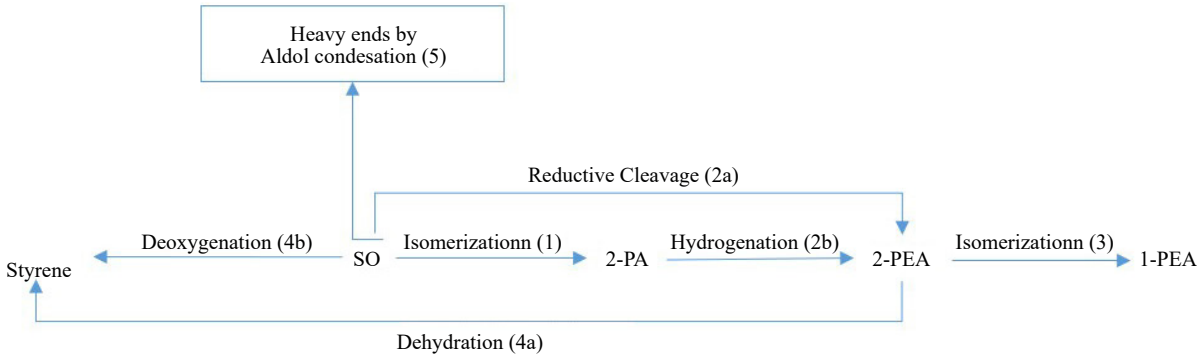

Figure 8. Reaction scheme for transformation of styrene oxide

With reference of Figure 8: Styrene oxide isomerizes to PAA on oxide catalysts which do not contain reducible active metals such as Ni, Co, Cu, Pd or Pt [3-13]. Kirm et.al [3] also attribute isomerization of 2-PEA to 1-PEA to the oxide carriers used in their study. Thus, these isomerization reactions are catalyzed by acid-base function. Hydrogenation of styrene oxide to 2-PEA on the other hand requires reducible active metals [3, 4, 14, 18, 19]. Thus, it is catalyzed by metal function. Trends in transformation of styrene oxide over the Ni, Co and Cu supported catalysts of the present study are presented below.

5.7.1 *Trends of catalyst activity:*

Trends of conversion with time on stream are shown in Figure 9 a, b, c for the Cobalt, Nickel and Copper based catalysts.

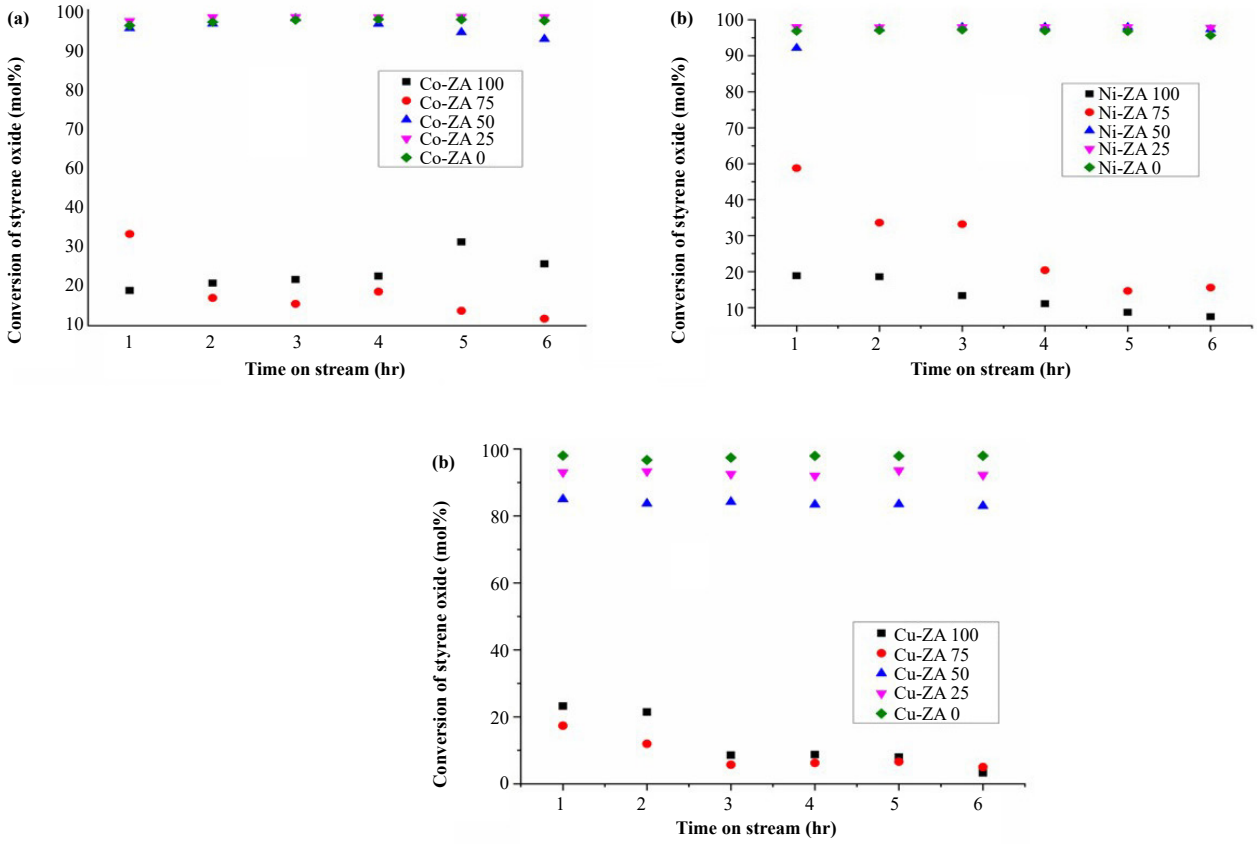

Figure 9. Conversion of styrene oxide on a) Co-catalysts b) Ni-catalysts c) Cu-catalysts supported on zirconia-alumina

As seen from Figure 9 a, b, c there is a clear trend of conversion with zirconia content of the catalyst. All the catalysts containing ≥ 75 mol% of zirconia in the zirconia-alumina carrier composition show poor initial conversion accompanied by some deactivation.

Trend of XPS area for surface concentration of active metals is shown in Figure 10 below. As seen from this Figure active metals are not detected in catalysts based on neat zirconia carrier (100% ZrO_2). These are Ni-ZA-100, Co-ZA-100 and Cu-ZA-100. Surface concentration of all three active metals improves with decreasing zirconia content (50 mol% ZrO2, Ni-ZA 50, Co-ZA 50 and Cu-ZA 50) and it is maximum on the surface of the neat alumina support (ZrO_2 0%), Ni-ZA-0, Co-ZA-0 and Cu-ZA-0.

Thus, the trend of activity directly correlates with surface concentration of active metals on the surface of the support. Changes in surface concentration of active metals affects reductive cleavage of styrene oxide and hydrogenation of PAA to 2-PEA both of which are catalyzed by metal function, thus affecting conversion.

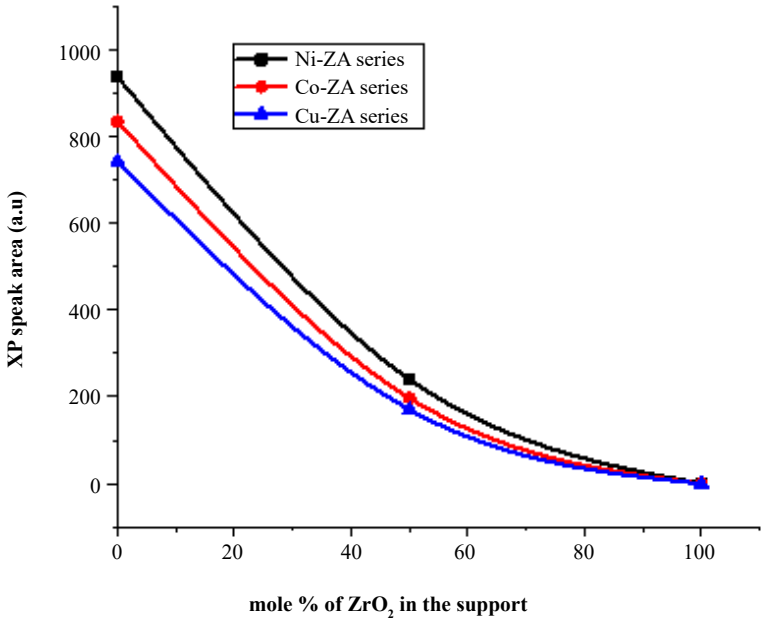

Figure 10. Surface concentrations of Co, Ni and Cu as a function of zirconia content of the supports used to prepare the catalysts.

5.7.2 *Trends of Space Time Yield (STY) of 2-PEA, PAA and PAA+2-PEA:*

PAA is formed by isomerization of styrene oxide (reaction 1 in reaction scheme Figure 8), which is catalyzed by acid function of catalysts. 2-PEA is formed by reductive cleavage of SO (reaction 2a in scheme) which requires a metal function. This reaction is in parallel to the isomerization of SO to PAA. 2-PEA can also form by a two-step sequential reaction viz. isomerization of SO to PAA (reaction 1 Figure 8), which is an acid catalyzed reaction, followed by the hydrogenation of PAA (reaction 2b Figure 8) which is catalyzed by metal function. A comparison of space time yields of PAA, 2-PEA provides insight of the influence of acid and metal functions of the catalysts for these reactions.

Space time yield is calculated from the space velocity of styrene oxide feed, its conversion and selectivity to a given product at steady state conversion as:

$$(STY)_i = (F/W)_{SO} * \text{fractional conversion of Styrene oxide} * \text{fractional selectivity of product i}$$

Where $(F/W)_{SO}$ is space velocity of styrene oxide feed to the reactor.

A comparison of STY of PAA, 2-PEA and combined STY of PAA+2-PEA of the catalysts is provided in Figure 11 below. The catalysts are arranged in decreasing order of zirconia content for a given active metal in the plot.

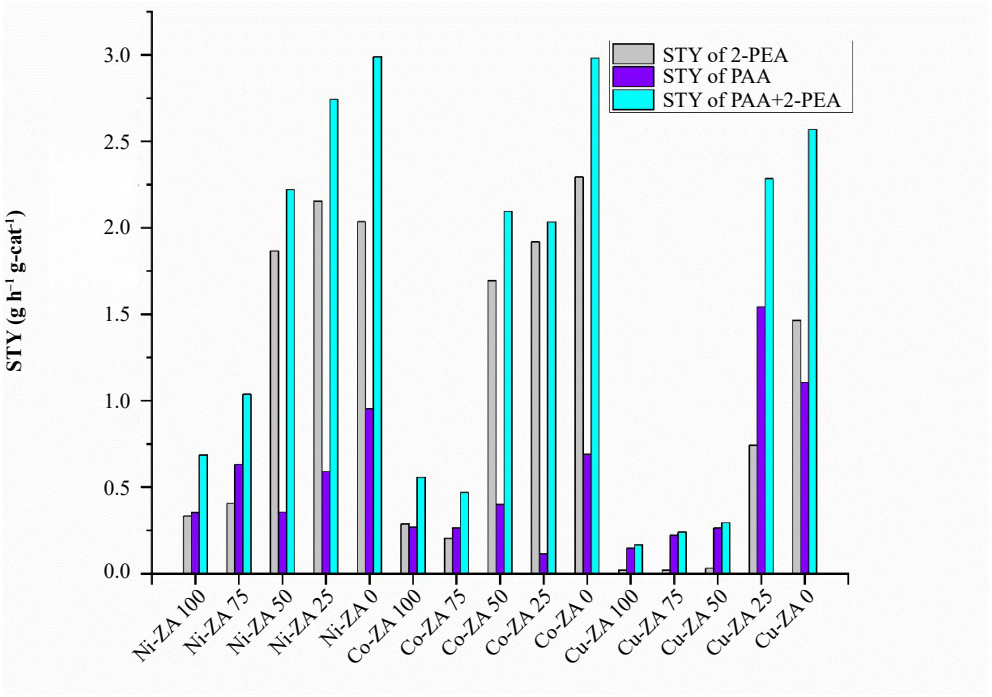

Figure 11. Space Time Yields of 2-PEA, PAA and (PAA+2-PEA) on Co, Ni and Cu catalysts supported on zirconia-alumina

As seen from Figure 11 above, the STY of both PAA and 2-PEA show an (inverse) increasing trend with decreasing zirconia content of catalyst. However, excepting for Cu-ZA 50, a sudden jump in STY of 2-PEA is observed when the zirconia content of the support used to prepare the catalysts is 50 mol% or lower. This is attributed to the following reasons. At high Zirconia content ≥75 mol% both strong acidity (Figure 12 below) and surface concentrations of active metals (Figure 10 above) are low. Trend of strong acidity of the catalysts is overlaid with STY of PAA in Figure 12 below.

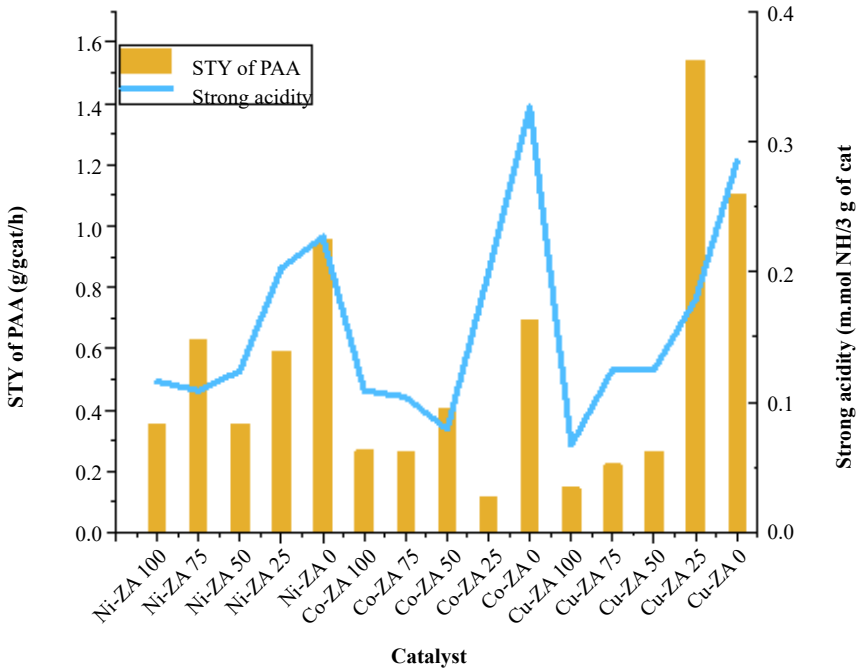

Figure 12. Trend of STY of PAA and strong acidity by NH_3-TPD

The catalysts are arranged in decreasing order of zirconia content for a given metal (Ni, Co or Cu) on the X axis. As seen from this Figure there is a positive correlation of strong acidity of the catalysts with STY of PAA. Thus the isomerization of SO to PAA is catalysed by the acid function of the catalyst. This is consistent with observations reported in literature [3-13]. It is also apparent that acidity is inversely related to zirconia content of the catalyst.

2-PEA is formed by reductive cleavage of SO (reaction 2a in Figure 8) which requires a metal function. 2-PEA can also form by a two-step sequential reaction viz. isomerization of SO to PAA (reaction 1 Figure 8), which is an acid catalyzed reaction, followed by the hydrogenation of PAA (reaction 2b Figure 8) which is catalyzed by metal function. Thus, this latter route requires a combination of both acid and metal functions. Since both acidity and surface concentrations of active metals are low when zirconia content of support is ≥75 mole% (as explained above), both routes are drastically affected resulting in significantly low STY of 2-PEA (Figure 11 above). This also results in the values of STY of PAA and 2-PEA being close to each other for Ni and Co catalysts with high zirconia content (≥75 mol% ZrO_2). STY of PAA is affected due to low acidity. These trends are irrespective of active metal Co, Ni or Cu.

Unlike in the case of Co and Ni catalysts, the STY of PAA in Cu catalysts with ZrO_2 content ≥50 mol% is significantly higher than that of 2-PEA. Cu-ZA 0 (where there is no zirconia in the catalyst) is the only exception. Thus, compared to its Co or Ni counterparts, zirconia significantly decreases the activity of copper towards hydrogenation reactions which form 2-PEA.

The difference in behaviour of Cu catalysts may also be attributed to the difference in its electronic configuration from that of Co or Ni as mentioned in the introduction section and highlighted in section 5.7.3

Thus, the Cu based catalysts on zirconia rich carrier have a poor hydrogenation function compared to the Co or Ni based catalysts. Psaro and Ravasio [3] have shown in batch reaction studies of hydrogenation of styrene oxide in dioxane that increasing zirconia (from Zr:Si 1 to 4.7) in SiZr supports, favors the formation of PAA (selectivity increases from 2% to 66%) relative to 2-PEA (which decreases from 80% to 14%) in 8% Cu/SiZr catalyst. Thus, higher zirconia favors formation of PAA relative to 2-PEA at the same active metal content. Their results also show that decreasing Cu content from 8% to 5% on silica doped with 1 wt% zirconia lowers selectivity of 2-PEA from 80% to 8% with concomitant increase in selectivity of PAA from 2% to 33%. Thus, hydrogenation function is strongly dependent on availability of Cu. The results of the present study show that Cu/zirconia-alumina supports with high zirconia content favor the formation of PAA similar to results of Psaro et.al. Hence, the combination of Cu and zirconia appears to have a similar effect in both silica and alumina carriers.

In the current study XPS studies show that the surface concentration of active metals in the catalysts decreases with increasing zirconia content (Figure 10) which reflects in their poor hydrogenation activity (low STY of 2-PEA in Figure 11). Thus, availability/accessibility of active metal is important. The results of the current study are in agreement with those of Psaro et al. in this respect.

5.7.3 *Trends of side reactions – Relative selectivity between formation of styrene and formation of 2-PEA:*

From the reaction scheme in Figure 8 it is seen that styrene and 2-PEA can form from styrene oxide by parallel reactions. Styrene can form by reaction 4b (deoxygenation). Styrene can also form from 2-PEA by reaction 4a (dehydration) provided the catalysts are acidic. 2-PEA forms from reaction 2a (reductive cleavage of SO) or reaction 1 (isomerization to PAA) followed by reaction 2b (hydrogenation of PAA). Formation of styrene and ethylbenzene has been reported by Hoelderich et.al. [33] over copper loaded on zeolitic supports and by Kirm et.al. [19] with 2 wt% Pt supported on carriers such as γ-alumina, MgO and activated carbon. Psaro et.al. [3] also report their formation in batch reactor studies over copper supported on silica, silica-alumina and silica-zirconia.

Formation of styrene is attributed to deoxygenation of styrene oxide by Sasu et.al.(nickel hydrotalcites) [4], Miyano et.al. (metal halides with Zn-Cu couple) [36] and Kinjenski et.al.(thermally dehydrated MgO) [37]. Sooknoi and Dwyer [38], Lange and Otten [39] attribute formation of styrene to dehydration of 2-PEA over acid sites on metal free oxide catalysts and zeolites. Jixiang Chen et.al [46] report that spillover hydrogen at interface of intermetallic Ni3Ga and SiO_2 support leads to hydrodeoxygenation of anisole to benzene.

Styrene is observed to form in the current study. It can form either by the dehydration of 2-PEA or deoxygenation of Styrene oxide (reactions 4a or 4b in scheme 1 Figure 8 respectively). The relative selectivity of styrene to 2-PEA calculated for the Co, Ni and Cu catalysts is shown in Figures 13a, b and c.

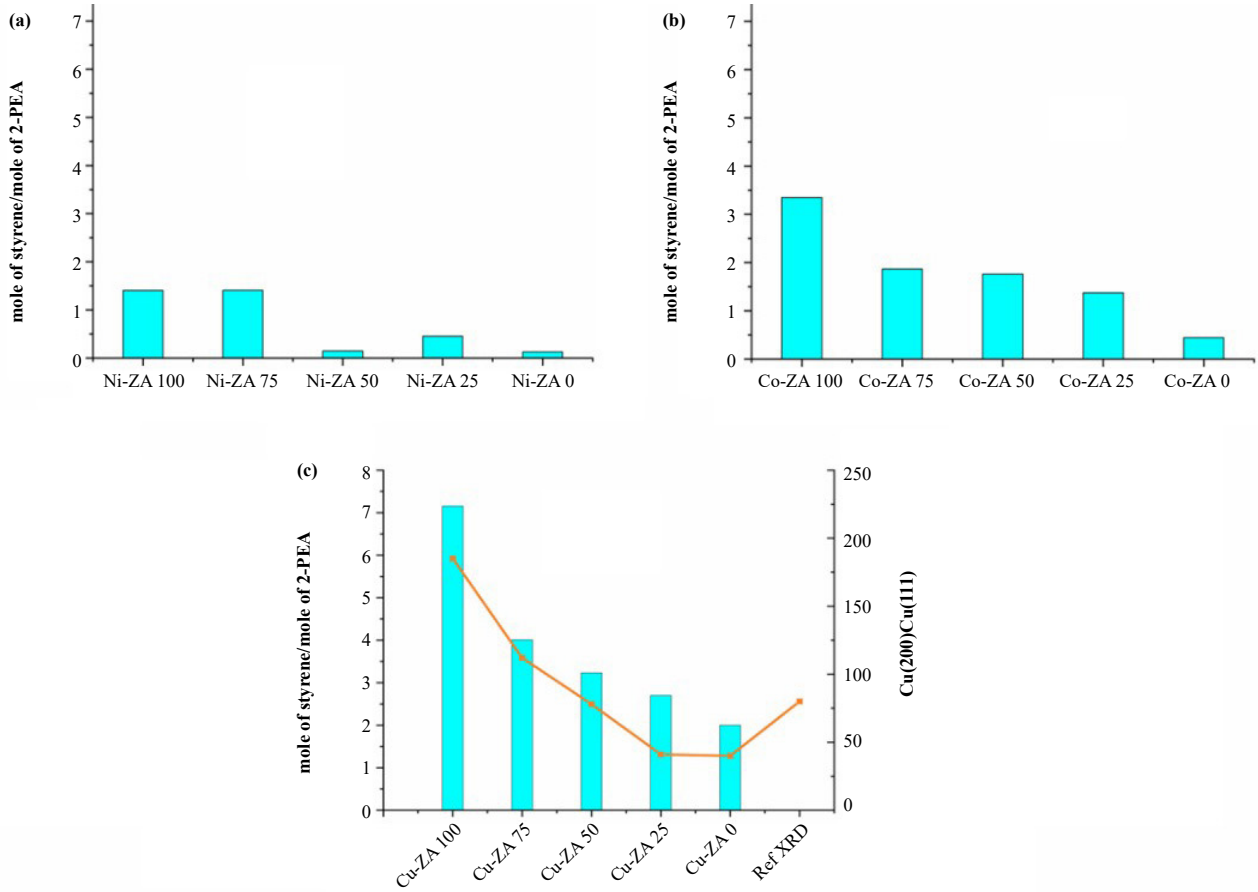

Figure 13. Relative selectivity between formation of styrene and 2-PEA on a) Co-catalysts b)Ni-catalysts c) Cu-catalysts supported on zirconia-alumina

As seen from Figure 13 a,b,c, the selectivity decreases with decreasing zirconia content for all three catalysts. As seen from these Figures, the trend for relative selectivity of Styrene:2-PEA is Cu >> Co > Ni catalysts. Interestingly, the copper based catalysts (Figure 13c) show 2 to 5-fold higher relative selectivity to styrene than their cobalt and nickel counterparts respectively. In order to understand the reason for this difference its relation with preferential orientation of Cu in reduced catalysts is examined (Figure 13c above).

The ratio of intensities of Cu(2 0 0) and Cu(1 1 1) XRD peak of reduced catalyst is overlaid on styrene selectivity in Figure 13c. As seen from this Figure catalysts with higher zirconia (≥75 mole%) content show a suppression of the Cu(1 1 1) plane of Cu, (which manifests as a higher value of the Cu(2 0 0)/Cu(1 1 1) ratio). Significantly higher selectivity to styrene is observed for these catalysts. Thus, suppression of the Cu(1 1 1) plane results in enhanced selectivity of styrene. Yu Jen Shih et.al. [53] have reported similar behavior of Cu(111) for the reduction of NOx to N2. They report that the rate constant for reduction of NOx increases by 20% when the Cu(200)/Cu(111) intensity ratio decreases from 60% to 30% (effectively increase in Cu(111)). Such preferential orientation is also reported for Cu 2 0 0/graphene [54] (for oxidation, reduction and coupling reactions).

Further, the catalysts which show higher selectivity to styrene have low strong acidity (Figure 12 above), hence, the formation of styrene by dehydration of 2-PEA (reaction 4a in Figure 8) is improbable, because dehydration is an acid catalyzed reaction. The product in these cases showed hazy appearance due to finely dispersed droplets of water which is a product of hydrodeoxygenation. Thus, our results are aligned with the formation of styrene by the hydrodeoxygenation of SO.

The strikingly different behavior of the copper catalysts may also be attributed to differences in electronic properties of these three active elements. The Fermi level not overlapping with the d band of Cu. It is 0.1 eV lower than the d band. Whereas, the d bands of both Ni and Co overlap with the Fermi level [55]. Quaino et.al. [55] have shown from model

Hamiltonian, quantum statistics and DFT calculations, that, an overlap of the d band and the Fermi level is one of three important criteria for good catalytic activity in hydrogen electrocatalysis.

Another contributor could be the difference in electronic properties of copper when compared to Ni or Co. Co, Ni and Cu are from the first transition series of the periodic table. The electronic configuration of Cu ($4s^1 3d^{10}$) shows anomalous behavior from that of Co ($4s^2 3d^7$) and Ni ($4s^2 3d^8$) in that, the 3d orbital is completely filled before the 4s orbital, which is half filled. The Allen scale electronegativity increases from Sc (1.19) to Co (1.84) and Ni (1.88) and then decreases for Cu (1.85) and Zn (1.59). The Pauling scale also shows a similar trend. Cu tends to have I and II (lower) oxidation states, where as Co tends to have II, III, IV, V and Ni II, III, IV (higher) oxidation states. Oxides of lower oxidation states tend to have more ionic character and hence tend to have basic chemical character [56].

Small quantities of ethylbenzene (EB) and toluene were also detected in the products. EB is expected to form by the hydrogenation of styrene.

Trace amounts of toluene were also observed in the products of all the samples. Formation of toluene is also reported by Hoelderich et.al. [33] who have studies Cu supported on zeolites. This is reported to form by hydrogenolysis of ethylbenzene [57].

Kochkar et.al. [5] report deactivation due to aldolization on basic catalysts resulting in the formation of 1,3,5-triphenylbenzene which leads to fouling. Deactivation by trimerization of PAA is reported on strongly acidic catalysts (zeolites) [9].

Trend of selectivity for heavy product was (Ni catalysts (2-8 mol%) < Co catalysts (7-16 mol%) < Cu catalysts (7-22 mol%). It may be responsible for deactivation of the catalyst with higher zirconia content. Considering the low acidity of catalysts of this study its formation is attributed to aldolization reactions.

5.7.4 *Trends of isomerization of 2-PEA to 1-PEA:*

2-PEA is the desired isomer. Trends of positional isomer selectivity of 2-PEA:1-PEA are shown in Figures 14 a, b, and c for the cobalt, nickel and copper based catalysts.

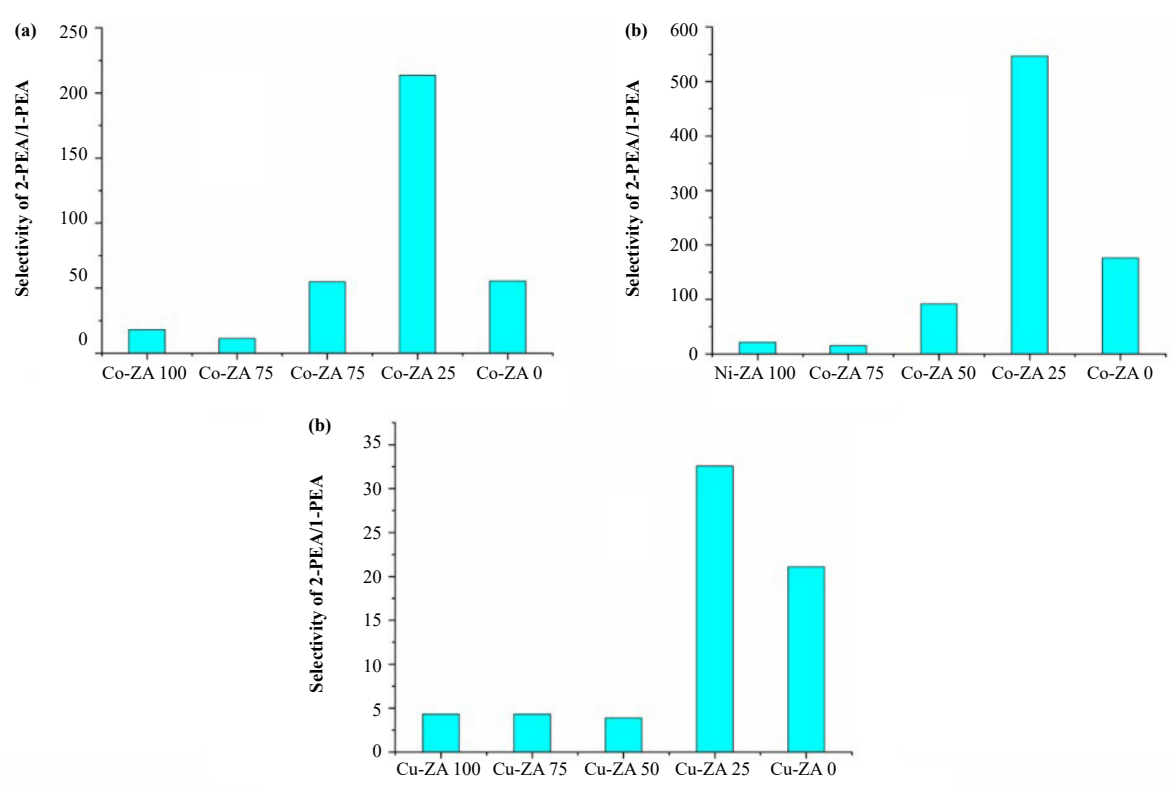

Figure 14. Positional isomer selectivity of PEA on a) Co-catalysts b)Ni-catalysts c) Cu-catalysts supported on zirconia-alumina

Kirm et.al. [19] have reported formation of 1-PEA in addition to 2-PEA over 2 wt% Pt supported on γ-Al_2O_3, activated carbon and MgO carriers, whereas they report that it is not detected in the case of 2 wt% Pd on MgO [18]. In the current study formation of small quantities of 1-PEA (undesired isomer) is observed in all the samples. Samples with higher alumina content show significantly lower selectivity to 1-PEA. Alumina is amphoteric in character. As seen from Figures 14 a, b and c catalysts prepared with carrier containing 25 mol% zirconia give significantly higher selectivity to desired isomer (2-PEA) within a given active metal series. Cu-ZA 0 is an exception. Between the metals the trend of isomer selectivity to 2-PEA is Ni-ZA 25 >> Co-ZA 25 >> Cu-ZA 25 ~ Cu-ZA 0.

The used catalysts were regenerated by controlled calcination in a mixture of air and N_2. The conversion of styrene oxide for three cycles was 96.0, 95.0 and 95.5% respectively with comparable product selectivity over all three cycles. Hence the catalysts are deemed regenerable.

6. Conclusion

Deposition-precipitation of zirconia on γ-Al_2O_3 significantly improves properties such as specific surface area and pore volume of the bi-component catalysts relative to catalysts based on neat zirconia. However, there are limitation at high zirconia content.

Unusual behavior is observed with respect to surface concentration of active metals and acidity. Increasing the concentration of deposited zirconia affects conversion of styrene oxide and STY of 2-PEA due to a decrease in surface concentrations of active metals which in turn affects metal function (hydrogenation). It also affects STY of PAA due to decrease in acidity since PAA forms by isomerization of SO which is an acid catalyzed reaction. Between the three metals, Nickel and Cobalt catalysts give the best space time yields for both 2-PEA alone and PAA + 2-PEA combined. Cu catalysts exhibit lowest STY for 2-PEA due to poor hydrogenation function which could be due to differences in its electronic properties relative to Co and Ni.

Copper shows a different behavior than Co and Ni catalysts in that it shows stronger metal-support interaction with zirconia whereas Co and Ni show stronger interaction with alumina. This reflects in their XRD crystallite sizes. It also shows preferred orientation by way of decrease in intensity of its 1 1 1 plane in zirconia rich catalysts. This correlates with the increased selectivity of styrene at the expense of 2-PEA. Styrene appears to form by deoxygenation of SO.

While non-noble metals are attractive from cost perspective they show lower selectivity than noble metal catalysts. Formation of styrene by-product needs to be suppressed significantly in non-noble metal based catalyst to improve yields of PAA and 2-PEA. The results show that increasing acidity of the catalysts helps in this respect. The results provide insights for further improvement of these catalysts. Multi-component catalysts which have potential for tuning both acid-base and metal functions could be explored in future.

Acknowledgement

The authors thank management of Sud-Chemie India Pvt. Ltd, Nandesari, Vadodara, India for providing facilities to carry out this work. The authors are grateful to the R&D management and Scientists from Analytical Department of Hindustan Petroleum Green R&D Centre, Bengaluru for Raman spectroscopy of the catalyst samples. The authors acknowledge support and encouragement provided by the Department of Applied Chemistry, The Maharaja Sayajirao University of Baroda.

Conflict of interest

There are no competing interests to declare.

Appendix

Transformation of Styrene oxide on bi-functional Ni, Co and Cu catalysts supported on zirconia-alumina

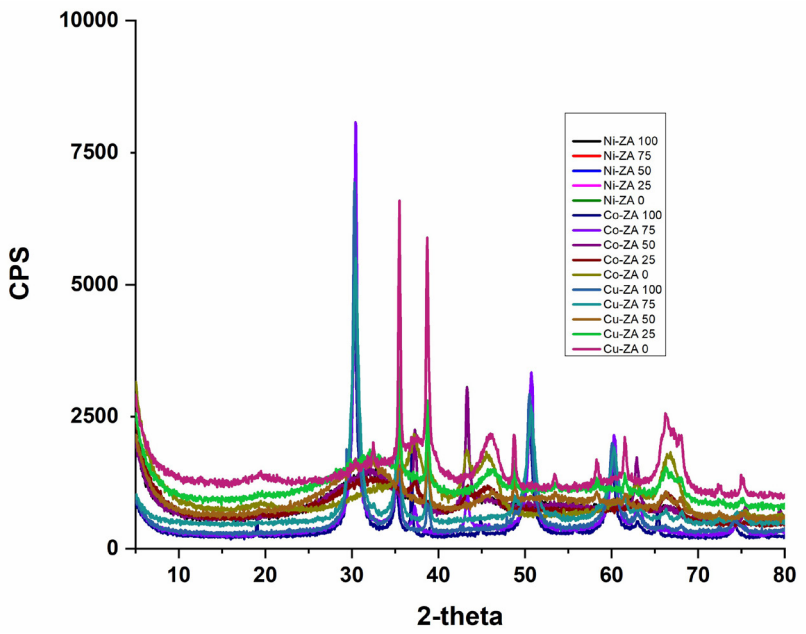

Figure A1. XRD of supported Ni, Co and Cu catalysts

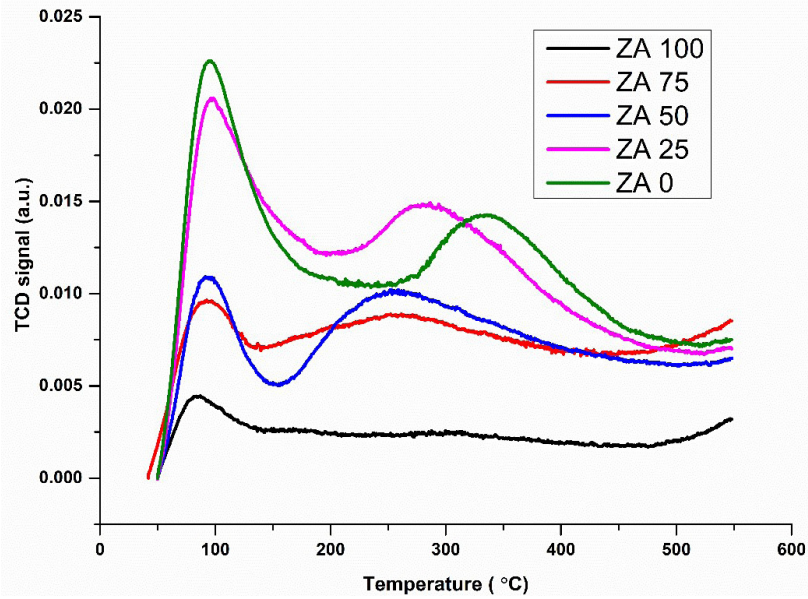

Figure A2. Ammonia TPD of supports used for preparation of Ni, Co and Cu supported metal catalysts

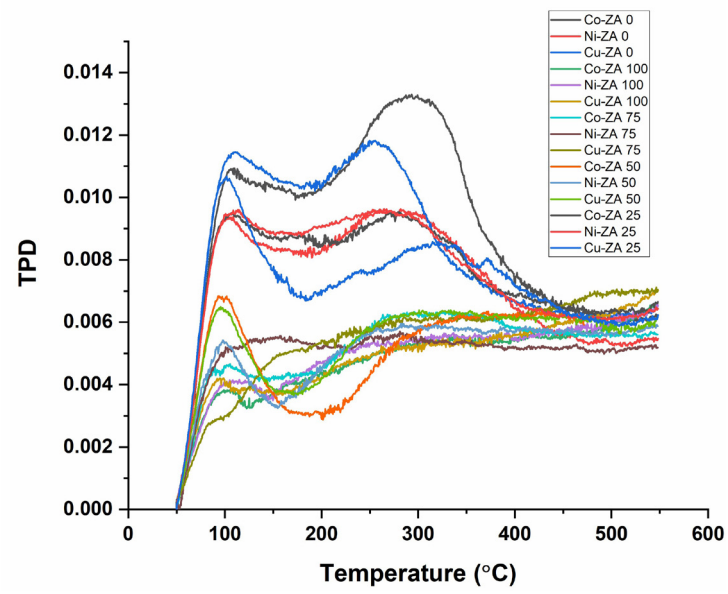

Figure A3. Ammonia TPD of Ni, Co and Cu supported metal catalysts

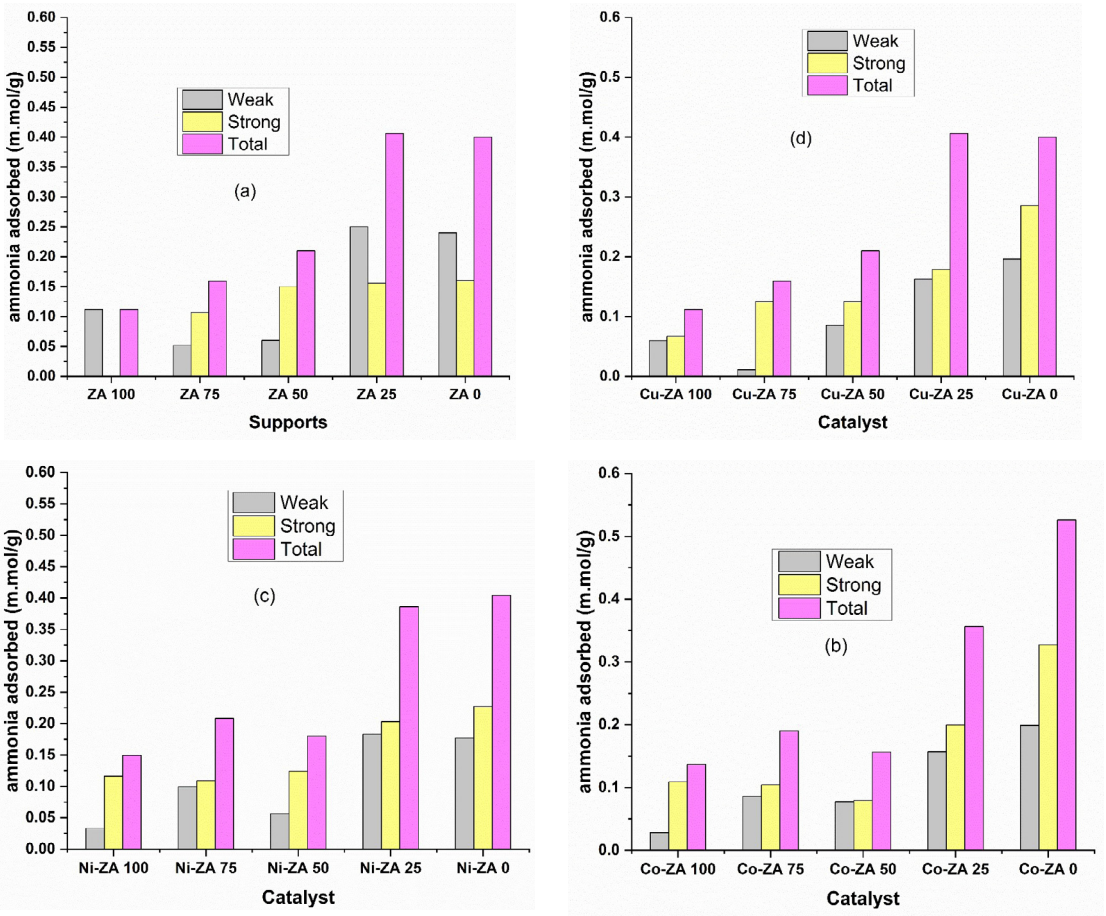

Figure A4. Weak, strong and total acidity of supports and corresponding Ni, Co and Cu supported metal catalysts a: Trend of acidity of neat supports; b: Trends of acidity of supported Co catalysts; c: Trend of acidity of supported Ni catalysts; d: Trend of acidity of supported Cu catalysts

References

[1] Olah GA, Reddy VP, Prakash GKS. Friedel-Crafts reactions. *Kirk-othmer encyclopedia of chemical technology*. Volume 11, 4th ed. John wiley & sons, New York; 1994. p.1042-1081

[2] Unuigboje A, Emenike B. Convergent preparation of 2-phenylethanol. *African J. pure Appl Chem*. 2011;5(6):123–6. http://www.academicjournals.org/AJPAC

[3] Zaccheria F, Psaro R, Ravasio N, Sordelli L, Santoro F. Mono and bifunctional catalysts for styrene oxide isomerization or hydrogenation. *Catal Letters*. 2011;141(4):587–91. https://doi.org/10.1007/s10562-010-0543-5

[4] Sasu A, Dragoi B, Ungureanu A, Royer S, Dumitriu E, Hulea V. Selective conversion of styrene oxide to 2-phenylethanol in cascade reactions over non-noble metal catalysts. *Catal Sci Technol*. 2016;6(2):468–78. Available from: http://xlink.rsc.org/?DOI=C5CY00779H

[5] Kochkar H, Clacens JM, Figueras F. Isomerization of styrene epoxide on basic solids. *Catal Letters*. 2002;78(1–4):91–4. https://doi.org/10.1023/A:1014914207019

[6] Costa V V., da Silva Rocha KA, Kozhevnikov I V., Gusevskaya E V. Isomerization of styrene oxide to phenylacetaldehyde over supported phosphotungstic heteropoly acid. *Appl Catal A Gen*. 2010 Jul;383(1–2):217–20. https://linkinghub.elsevier.com/retrieve/pii/S0926860X10004126

[7] Gou M-L, Wang R, Qiao Q, Yang X. Effect of mesoporosity by desilication on acidity and performance of HZSM-5 in the isomerization of styrene oxide to phenylacetaldehyde. *Microporous Mesoporous Mater*. 2015 Apr;206:170–6. https://linkinghub.elsevier.com/retrieve/pii/S138718111400688X

[8] Gou ML, Wang R, Qiao Q, Yang X. Effect of phosphorus on acidity and performance of HZSM-5 for the isomerization of styrene oxide to phenylacetaldehyde. *Appl Catal A Gen*. 2014;482:1–7. http://dx.doi.org/10.1016/j.apcata.2014.05.023

[9] Gou M-L, Cai J, Song W, Liu Z, Ren Y-L, Pan B, et al. Coking and deactivation behavior of ZSM-5 during the isomerization of styrene oxide to phenylacetaldehyde. *Catal Commun*. 2017 Jul;98:116–20. https://linkinghub.elsevier.com/retrieve/pii/S156673671730170X

[10] Zhang X-F, Yao J, Yang X. Effects of crystal size and pore structure on catalytic performance of TS-1 in the isomerization of styrene oxide to phenyl acetaldehyde. *Microporous Mesoporous Mater*. 2017 Jul;247:16–22. https://linkinghub.elsevier.com/retrieve/pii/S138718111730224X

[11] Zhang X-F, Yao J, Yang X. Isomerization of Styrene Oxide to Phenyl Acetaldehyde over Different Modified Beta Zeolites. *Catal Letter*s. 2017 Jun 6;147(6):1523–32. http://link.springer.com/10.1007/s10562-017-2004-x

[12] Qiao Q, Wang R, Gou M, Yang X. Catalytic performance of boron and aluminium incorporated ZSM-5 zeolites for isomerization of styrene oxide to phenylacetaldehyde. *Microporous Mesoporous Mater*. 2014;195:250–7. https://doi.org/10.1016/j.micromeso.2014.04.042

[13] Chareonsiriwat L, Chavasiri W. Convenient method for the transformation of epoxide to aldehyde and acetonide mediated by Cr-PLM. *Synth Commun*. 2017 Feb 16;47(4):257–67. https://www.tandfonline.com/doi/full/10.1080/00397911.2016.1254799

[14] Poondi D, Vannice MA. The influence of MSI (metal-support interactions) on phenylacetaldehyde hydrogenation over Pt catalysts. *J Mol Catal A Chem*. 1997 Sep;124(1):79–89. https://linkinghub.elsevier.com/retrieve/pii/S1381116997000666

[15] Wood TF. Process for preparing beta-phenyl ethyl alcohol. *US Patent 2524096A*, 1950.

[16] Gibson CA, Louis Foster Theiling J. Hydrogenation of styrene oxide to produce 2-phenylethanol. *US 4064186*, 1977.

[17] Vasanti G.Yadav and, Chandalia SB. Synthesis of Phenethyl Alcohol by Catalytic Hydrogenation of Styrene Oxide. *Org Process Res Dev*. 1998 Sep 1;2(5):294–7. https://pubs.acs.org/doi/10.1021/op980027r

[18] Kirm I, Medina F, Rodríguez X, Cesteros Y, Salagre P, Sueiras JE. Preparation of 2-phenylethanol by catalytic selective hydrogenation of styrene oxide using palladium catalysts. *J Mol Catal A Chem*. 2005;239(1–2):215–21. https://doi.org/10.1016/j.molcata.2005.06.032

[19] Kirm I, Medina F, Sueiras JE, Salagre P, Cesteros Y. Hydrogenation of styrene oxide in the presence of supported platinum catalysts to produce 2-phenylethanol. *J Mol Catal A Chem*. 2007 Jan 2;261(1):98–103. https://linkinghub.elsevier.com/retrieve/pii/S1381116906010351

[20] Yadav GD, Lawate YS. Selective hydrogenation of styrene oxide to 2-phenyl ethanol over polyurea supported Pd–Cu catalyst in supercritical carbon dioxide. *J Supercrit Fluids*. 2011 Nov;59:78–86. https://linkinghub.elsevier.com/retrieve/pii/S0896844611003160

[21] Yadav GD, Lawate YS. Hydrogenation of Styrene Oxide to 2-Phenyl Ethanol over Polyurea Microencapsulated Mono- and Bimetallic Nanocatalysts: Activity, Selectivity, and Kinetic Modeling. *Ind Eng Chem Res*. 2013 Mar

20;52(11):4027–39. https://pubs.acs.org/doi/10.1021/ie302587j
[22] Bajaj HC, Hasan S, Abdi R, Kureshy RI, Khan NH, Asharafbhai A. Hydrogenation of styrene oxide forming 2-phenyl ethanol. Vol. 2. *US 9040755 B2*, 2015.
[23] Hossain, S.; Jalil MA. A Recyclable Heterogeneous Palladium Catalyst Anchored to Modified Metal-Organic Framework for Hydrogenation of Styrene Oxide. *Russ J Org Chem*. 55(12):1946–50. https://doi.org/10.1134/S1070428019120236
[24] Manríquez-Ramírez ME, San German CR, Flores ME, Valdez MT, Ortiz-Islas E. Styrene oxide hydrogenation reaction using Pt/TiO2-ZrO2-supported catalysts for 2-phenylethanol production. *Mater Res Bull*. 2020 Aug;128:110872. https://linkinghub.elsevier.com/retrieve/pii/S0025540819328442
[25] Viswanadhan M, Potdar A, Divakaran A, Badiger M, Rode C. Product distribution in hydrogenation of styrene oxide over Pd/chitosan catalyst. *Res Chem Intermed*. 2016 Oct 2;42(10):7581–95. http://link.springer.com/10.1007/s11164-016-2554-3
[26] Suzuki S. Hydrogenation of epoxides to primary alcohols. *US patent 3975449*, 1976.
[27] Ye R-P, Lin L, Li Q, Zhou Z, Wang T, Russel CK, et al. Recent progress in improving the stability of copper-based catalysts for hydrogenation of carbon-oxygen bonds. *Catal Sci Technol*. 8:3428–49 https://doi.org/10.1039/C8CY00608C.
[28] Nitta Y, Ueno K, Imanaka T. Selective hydrogenation of αβ-unsaturated aldehydes on cobalt silica catalysts obtained from cobalt chrysotile. *Appl Catal*. 1989 Jan;56(1):9–22. https://linkinghub.elsevier.com/retrieve/pii/S0166983400801554
[29] Ando C, Kurokawa H, Miura H. Selective hydrogenation of aldehyde groups in various α,β-unsaturated aldehydes over alumina-supported cobalt (0) catalyst. *Appl Catal A Gen*. 1999 Sep;185(2):L181–3. https://linkinghub.elsevier.com/retrieve/pii/S0926860X99001428
[30] Kanojiya SK, Patel A, Shukla G, Joshi N, Sharma P, Gupta PL, et al. Hydrogenation of styrene oxide to 2-phenyl ethanol over supported Nanonickel catalyst. *Int J Sci Eng Res*. 2015;6(2). https://www.citefactor.org/journal/pdf/Hydrogenation-of-styrene-oxide-to-2-phenyl-ethanol.pdf
[31] Kanojiya SK, Shukla G, Sharma S, Dwivedi R, Sharma P, Prasad R, et al. Hydrogenation of Styrene Oxide to 2-Phenylethanol over Nanocrystalline Ni Prepared by Ethylene Glycol Reduction Method. *Int J Chem Eng*. 2014;2014:1–6. http://www.hindawi.com/journals/ijce/2014/406939/
[32] Vicente I, Salagre P, Cesteros Y. Ni nanoparticles supported on microwave-synthesised saponite for the hydrogenation of styrene oxide. *Appl Clay Sci*. 2011 Aug;53(2):212–9. https://linkinghub.elsevier.com/retrieve/pii/S0169131710004412
[33] Hoelderich, Wolfgang F, Norbert Goetz W, Leopold Hupfer F. Preparation of phenylethanols. *US 4943667*, 1990.
[34] Bergadà O, Salagre P, Cesteros Y, Medina F, Sueiras JE. Control of the basicity in Ni-MgO systems: Influence in the hydrogenation of styrene oxide. *Catal Letters*. 2008;122(3–4):259–66. https://doi.org/10.1007/s10562-007-9373-5.
[35] Bergadà O, Salagre P, Cesteros Y, Medina F, Sueiras JE. Effective catalysts, prepared from several hydrotalcites aged with and without microwaves, for the clean obtention of 2-phenylethanol. *Appl Catal A Gen*. 2007 Jan;331:19–25. https://linkinghub.elsevier.com/retrieve/pii/S0926860X07004401
[36] Miyano S, Hida M, Hashimoto H. Deoxygenation of Styrene Oxide by Zinc Metal and Lewis Acid. *Bull Chem Soc Jpn*. 1969 Mar;42(3):746–9. http://www.journal.csj.jp/doi/10.1246/bcsj.42.746
[37] J Kinjenski, M Glinski JR. Hydrogen transfer over MgO. An alternative method for hydrogenation-dehydrogenation reactions. In: M Guisnet, J Barrault E al. (eds.) *Studies in Surface Science and Catalysis*. 1988. p. 231–40.
[38] Tawan Sooknoi JD. Hydrogenation of styrene and hydrogenolysis of 2-PEA; Mechanistic study of side chain alkylation of toluene and methanol. In: Laurent Bonneviot SK, (eds.). Studies in Surface Science and Catalysis Vol 97;Zeolites: A refined tool for designing catalytic sites; *Proceedings of International zeolite symposium*. Quebec Canada; 1995. p. 426.
[39] LANGE J, OTTEN V. Dehydration of phenyl-ethanol to styrene: Zeolite catalysis under reactive distillation. *J Catal*. 2006 Feb 15;238(1):6–12. https://linkinghub.elsevier.com/retrieve/pii/S0021951705004641
[40] Pathan RH, Modi CK, Basrur A. Effect of pH on the detailed chemical nature and metal-carbonate species in as synthesized zirconia alumina composites. *J Am Ceram Soc*. 2020 Nov;103(11):6615–29. https://onlinelibrary.wiley.com/doi/10.1111/jace.17368
[41] Olusola OJ, Sudip M. Temperature programme reduction (TPR) studies of cobalt phases in -alumina supported cobalt catalysts. *J Pet Technol Altern Fuels.* 2016 Jan 31;7(1):1–12. http://academicjournals.org/journal/JPTAF/article-abstract/9824F0256972
[42] Li J, Lu G, Wu G, Mao D, Wang Y, Guo Y. Promotional role of ceria on cobaltosic oxide catalyst for low-temperature CO oxidation. *Catal Sci Technol*. 2012;2(9):1865. http://xlink.rsc.org/?DOI=c2cy20118f

[43] McTAGGART FK. Reduction of Zirconium and Hafnium Oxides. *Nature*. 1961 Sep;191(4794):1192–1192. https://www.nature.com/articles/1911192a0
[44] Hoang D-L, Berndt H, Lieske H. Hydrogen spillover phenomena on Pt/ZrO2. *Catal Letters*. 1995 Jun;31(2–3):165–72. http://link.springer.com/10.1007/BF00808830
[45] Jung K-D, Bell AT. Role of Hydrogen Spillover in Methanol Synthesis over Cu/ZrO2. *J Catal*. 2000 Jul;193(2):207–23. https://linkinghub.elsevier.com/retrieve/pii/S0021951700928811
[46] Zheng Y, Zhao N, Chen J. Enhanced direct deoxygenation of anisole to benzene on SiO2-supported Ni-Ga alloy and intermetallic compound. *Appl Catal B Environ*. 2019 Aug;250:280–91. https://linkinghub.elsevier.com/retrieve/pii/S0926337319301973
[47] Mironova-Ulmane N, Kuzmin A, Sildos I, Puust L, Grabis J. Magnon and Phonon Excitations in Nanosized NiO. *Latv J Phys Tech Sci*. 2019 Apr 1;56(2):61–72. https://www.sciendo.com/article/10.2478/lpts-2019-0014
[48] Meza Fuentes E, Rodriguez Ruiz JI, Rangel Santos M do C. Characteristics of NiO present in solids obtained from hydrotalcites based on Ni/Al and Ni-Zn/Al. *DYNA*. 2019 Jul 1;86(210):58–65. https://revistas.unal.edu.co/index.php/dyna/article/view/78559
[49] Rashad M, Rüsing M, Berth G, Lischka K, Pawlis A. CuO and Co 3 O 4 Nanoparticles: Synthesis, Characterizations, and Raman Spectroscopy. *J Nanomater*. 2013;2013:1–6. http://www.hindawi.com/journals/jnm/2013/714853/
[50] Hadjiev VG, Iliev MN, Vergilov I V. The Raman spectra of Co3O4. *J Phys C Solid State Phys*. 1988 Mar 10;21(7):L199–201. https://iopscience.iop.org/article/10.1088/0022-3719/21/7/007
[51] Naumenko AP, Berezovska N, Biliy MM, Shevchenko O V. Vibrational analysis and Raman spectra of tetragonal zirconia. *Phys Chem Solid state*. 2008;9(1):121–5. https://www.researchgate.net/publication/285329926
[52] Wachs IE, Hardcastle FD, Chan SS. Raman spectroscopy of supported metal oxide catalysts. *Spectroscopy*. 1986;1(8):30–8.
[53] Shih Y-J, Wu Z-L, Lin C-Y, Huang Y-H, Huang C-P. Manipulating the crystalline morphology and facet orientation of copper and copper-palladium nanocatalysts supported on stainless steel mesh with the aid of cationic surfactant to improve the electrochemical reduction of nitrate and N2 selectivity. *Appl Catal B Environ*. 2020 Sep;273:119053. https://linkinghub.elsevier.com/retrieve/pii/S0926337320304689
[54] Primo A, Esteve-Adell I, Blandez JF, Dhakshinamoorthy A, Álvaro M, Candu N, et al. High catalytic activity of oriented 2.0.0 copper(I) oxide grown on graphene film. *Nat Commun*. 2015;6(4). https://doi.org/10.1038/ncomms9561
[55] Quaino P, Juarez F, Santos E, Schmickler W. Volcano plots in hydrogen electrocatalysis-uses and abuses. Vol. 5, *Beilstein Journal of Nanotechnology*. 2014. p. 846–54.
[56] Averill BA, Eldredge P. The d-block elements. *Principles of General Chemistry* (v 10). Ch 23. https://2012books.lardbucket.org/books/principles-of-general-chemistry-v1.0/index.html
[57] Hoangvan C. Hydrogenolysis of ethylbenzene over a supported nickel catalyst derived from nickel hydroaluminate. *J Catal* . 1987 Jun;105(2):469–77. https://linkinghub.elsevier.com/retrieve/pii/0021951787900741